MDPI

Article

Petrography and Provenance of the Sub-Himalayan Kuldana Formation: Implications for Tectonic Setting and Palaeoclimatic Conditions

Ahmer Bilal [1,2], Muhammad Saleem Mughal [2], Hammad Tariq Janjuhah [3,*], Johar Ali [2], Abrar Niaz [2], George Kontakiotis [4], Assimina Antonarakou [4], Muhammad Usman [2], Syed Asim Hussain [5] and Renchao Yang [1,6,*]

1   Shandong Provincial Key Laboratory of Depositional Mineralization & Sedimentary Minerals, Shandong University of Science and Technology, Qingdao 266590, China; ahmerbilal47@gmail.com
2   Institute of Geology, University of Azad Jammu and Kashmir, Muzaffarabad 13100, Pakistan; saleem.mughal@ajku.edu.pk (M.S.M.); jgeologist19@gmail.com (J.A.); abrar.niaz@ajku.edu.pk (A.N.); usmangeo3274@gmail.com (M.U.)
3   Department of Geology, Shaheed Benazir Bhutto University Sheringal, Dir (U) 18000, Pakistan
4   Department of Historical Geology-Paleontology, Faculty of Geology and Geoenvironment, School of Earth Sciences, National and Kapodistrian University of Athens, Panepistimiopolis, Zografou, 15784 Athens, Greece; gkontak@geol.uoa.gr (G.K.); aantonar@geol.uoa.gr (A.A.)
5   Department of Geosciences, University of Baltistan, Skardu 16100, Pakistan; s.asim@uobs.edu.pk
6   Laboratory for Marine Mineral Resources, Qingdao National Laboratory for Marine Science and Technology, Qingdao 266071, China
*   Correspondence: hammad@sbbu.edu.pk (H.T.J.); r.yang@sdust.edu.cn (R.Y.)

Abstract: In this paper, the depositional environment, age, and tectonic context of the Sub-Himalayan Kuldana Formation are discussed in detail. To determine the Kuldana Formation's depositional environment, age, and tectonic setting, sedimentological, palaeontological, and petrographic investigations have been conducted accordingly. The Kuldana Formation lithologically consists of both siliciclastic and carbonate rocks. Petrographically, the Kuldana Formation's sandstone is divided into litharenite and feldspathic litharenite petrofacies. The sandstone plots on the QtFL and QmFLt suggest that the sandstone of the Kuldana Formation derived from a recycled orogen provenance field that developed during the collision of the Indian and Eurasian plates in the Lesser and Higher Himalayas. The plots in the diamond diagram further demonstrate that the detritus of the Kuldana Formation was derived from low and middle-to-upper rank metamorphic rocks of the Himalayas. Throughout the deposition of sandstone, paleo-climate conditions were semi-humid to semiarid. Dolostone and limestone are the two main types of carbonate rocks found in the Kuldana Formation. According to Dunham's Classification, the Kuldana Formation limestone is classified as mudstone, wackstone, and packstone. These petrofacies suggest that the limestone was deposited in an inner-outer ramp setting. The bioclasts include bivalves, brachiopods, crinoid, gastropods, *Globigerinoides* spp., *Lockhartia pustulosa*, miliolids, *Nummulites atacicus*, *Nummulites discorbina*, *Nummulites mamillatus*, *Nummulites djodjokartae*, *Nummulites vascus*, and ostracods suggesting that the age of Kuldana Formation is Middle Eocene-early Oligocene. The Kuldana Formation was deposited during the initial stages of the Himalayan Orogeny as a result of the Ceno-Tethys Ocean's regression and transgression, as revealed by a succession of siliciclastic and non-clastic rocks.

Keywords: Ceno-Tethys Ocean; Kuldana Formation; petrofacies; provenance; regression; transgression; sandstones

1. Introduction and Geological Setting

The Himalayas were formed by the collision of the Indian and Eurasian plates during the Paleogene [1–3]. The Indian Plate traveled about 5000 km from south to north before

colliding with the Eurasian Plate around 55 million years ago (Ma) [4,5]. The Ceno-Tethys Ocean closed as a result of this continent-to-continent collision, and a new basin known as the Himalayan Foreland Basin (HFB) was formed [6–8]. The Himalayas are subdivided into three types, e.g., Higher Himalayas, Lesser Himalayas, and Sub Himalayas from north to south [9]. A thrust fault known as the Main Central Thrust (MCT) separates the Higher and Lesser Himalayas (Figure 1a). The Main Boundary Thrust (MBT) separates the Lesser Himalayas from the Sub-Himalayas/HFB, whereas the Salt Range Thrust (SRT) demarcates the Sub-Himalayas' southern boundary [10,11].
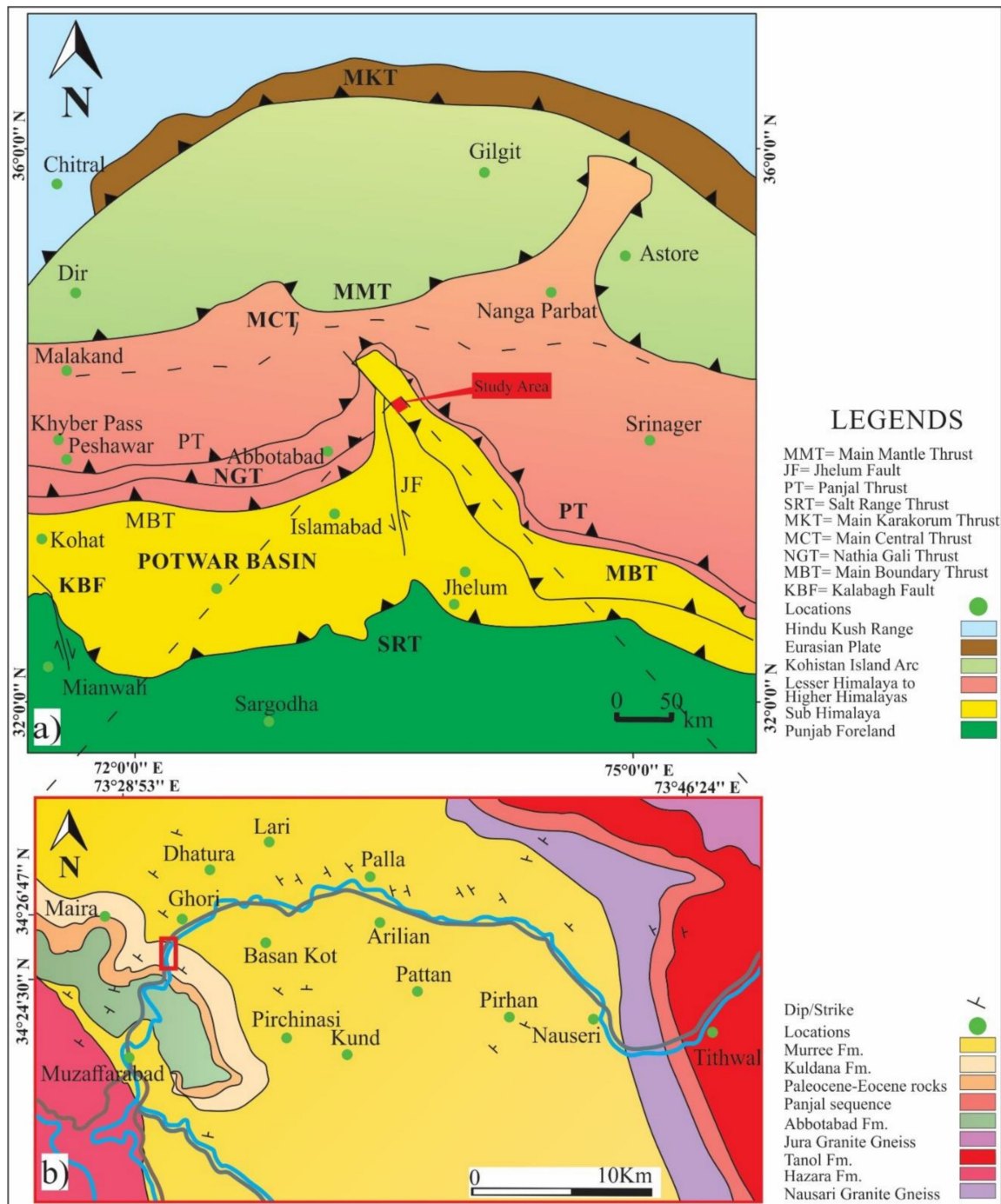

Figure 1. (**a**) A northern Pakistan's tectonic map; (**b**) a geological map of the Kuldana Formation in the Yadgaar Section Muzaffarabad area, showing sample locations.

Hazara Kashmir Syntaxis (HKS) is an antiformal structure that developed in the Sub-Himalayan region due to ongoing Himalayan Orogeny. HKS is comprised of older rocks in the limbs and younger rocks in its core [12,13]. As shown by steep slopes and locally anomalous terrain of the recycled orogen, HKS is an uplifted area [14,15]. The Yadgaar Section lies in the core of HKS (Figure 1b) and is bounded by latitudes and longitudes of 34°24′58″ N to 34°25′49″ N and 73°29′03″ E to 73°29′04″ E, respectively. The Yadgaar Section contains shallow marine-continental/fluvial sedimentary deposits of Cambrian-recent [16].

The boundary between the Paleocene and Eocene periods is marked by the ophiolitic and volcanic detritus that were deposited on the passive margins of India and Eurasian plates [17]. The collisional basins on both sides of the proto-Himalayan mountain range were filled with sediment after the rise of the mountain chain. The Early Eocene Chulung La Formation was deposited in the topmost portion of the "piggyback" basin (a small sedimentary sub-basin developed in the foreland basin, above a moving thrust sheet). In this Tethys Himalayan passive-margin succession, fluvial-deltaic red beds were deposited [13]. The red beds of the Eocene-Miocene quartzo lithic deltaic facies include sedimentary and low-grade metasedimentary material that derived from pro to Himalayan thrust sheets as well as volcanic-ophiolitic deposits associated with the suture zone. The subaerial foreland basins of the Indian continent are the distal analogs of the Neogene-aged Siwalik to the Quaternary molasses of the Indo-Gangetic Plain (Figure 2). They are underlain by the continent's crust [18]. Dickinson and Suczek [19] first developed the provenance system, and later Dickinson [20] refined it. The petrographic study of the detrital sandstone composition is an excellent approach to determining its tectonic settings, source type, and paleo-climatic conditions (Figures 3 and 4) [11,12,21–23].

The Paleogene rocks are divided into two groups: marine (shallow shelf) and transitional (deltaic). In the Yadgar Section, Muzaffarabad area, the total thickness of the Kuldana Formation is 1150 m (Figures 2, 3i and 5). The Kuldana Formation has a dis-conformable contact with the underlying Early Eocene Chorgali Formation [24–29] (Figure 4b), and is dominantly comprised of variegated-colored shales, siltstone, sandstones, and lenses of limestone. The upper contact of the Kuldana Formation is found unconformable with the Murree Formation (Figure 4d). Previous studies based on biostratigraphic investigations conducted in the Murree, Muzaffarabad, and Balakot districts dated the Kuldana Formation between 53 and 43 Ma (Early-Middle Eocene) [22,30]. The Eocene strata (~55–48 Ma) were deposited in a foredeep zone [12]. They further proposed that the detritus of these sediments was derived from the Kohistan–Ladakh arc (KLA), the Lhasa Block (LB), and the Karakoram Block (KB) of the Asian terrane. Previous researchers also recovered the fossils of vertebrates, foraminifers, bivalves, and gastropods from various sections of the Kuldana Formation [31–33].

The petrography of detrital sandstone rocks is an important method for determining siliciclastic rock provenance and pinpointing mineralogical composition. Accurate mineralogical calculations are critical in the petrological investigation of rocks containing clay deposits for engineering and industrial purposes [34]. The fundamental goal of sand-stone petrography is to determine the lithologic qualities of the source rocks and the tectonic context [19,21,35–37]. To recognize the tectonic settings of Himalayan strata, modal values were used [38,39]. The most important component in identifying provenance is understanding the tectonic settings [40,41]. Furthermore, the tectonic settings of sedimentary environments influence variables affecting sandstone composition, and some of these variables remain unchanged even after a long period of severe-tropical weathering. As a result, the composition of HFB sandstone is important for understanding the genesis of the orogenic belt, depositional environment, and geotectonic settings of the region. Kuldana Formation/Balakot Formation (Pakistan), Upper Subathu Group (Jammu and Kashmir and Himachal Pradesh, India), and Upper Bhainskati Formation (Nepal; Figure 2) [11,42].
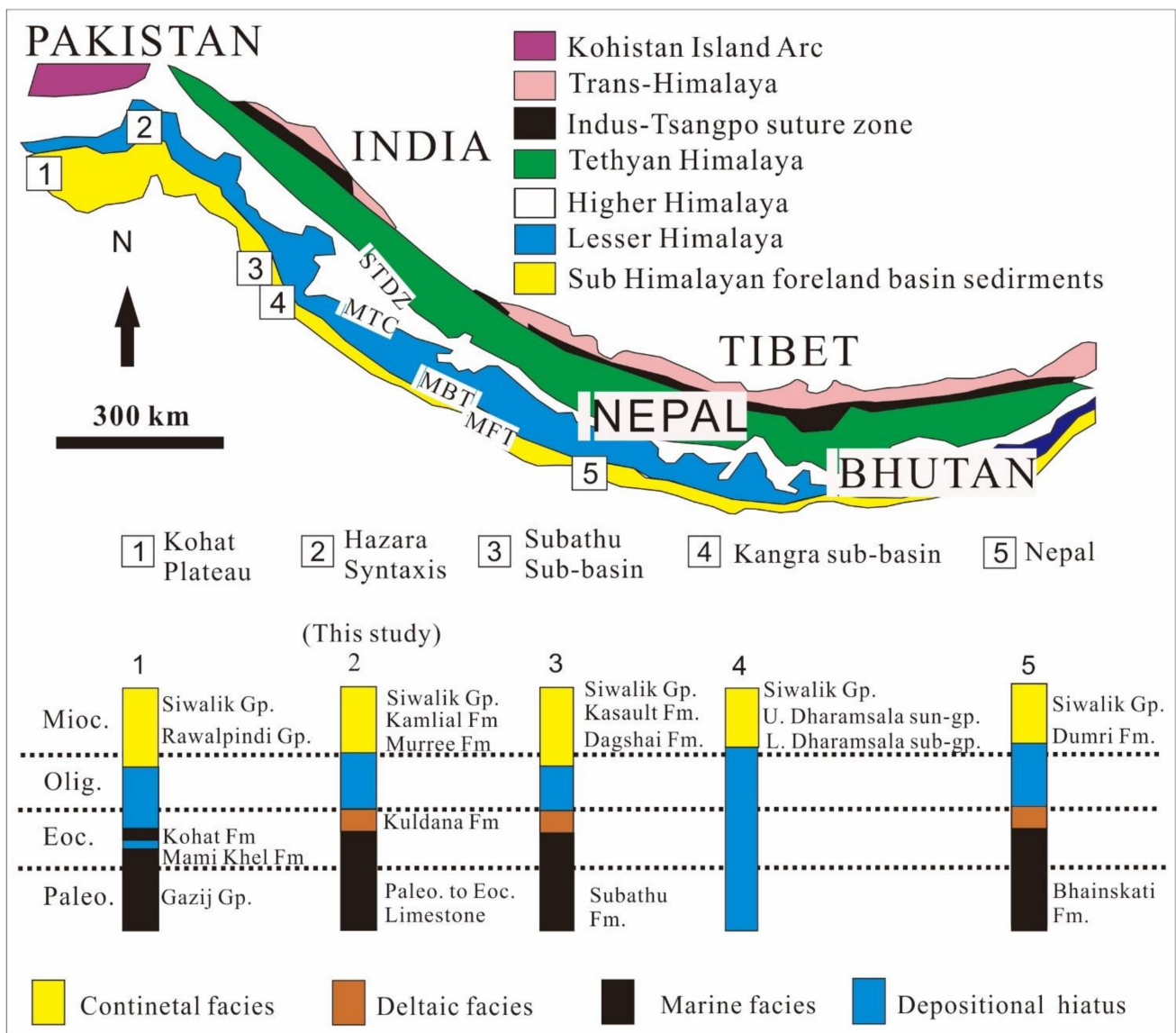
Figure 2. Outcrop locations and lithological correlation map of the Kuldana Formation with stratigraphic equivalent formations in the Himalayan range (Pakistan, India, and Nepal; Modified after 4). MBT, Main Boundary Thrust; MCT, Main Central Thrust; MFT, Main Frontal Thrust; STDZ, South Tibetan Detachment Zone.

Various geoscientists have studied the Kuldana Formation and its coeval Upper Subathu Group in the HFB to determine its provenance, tectonic development, and biostratigraphy [12,13,16,43]. However, they studied the Kuldana Formation and its coeval formations in different areas to determine its individual aspects. The depositional environment, age, and tectonic setting of the Kuldana Formation in the Yadgaar region have not yet been examined using a combined sedimentological and palaeontological approach with detailed mineralogical composition. The current study's goal is to determine the depositional environment, age, and tectonic setting of the area during the deposition of the Kuldana Formation by detailed sedimentological, palaeontological, and mineralogical investigations.

Figure 3. Photomicrograph showing (**a**) mudstone, (**b**,**l**) pencil-like shales, (**c**) variegated color shale, (**d**) reduction sports, (**e**) fine and coarse grain sandstone, (**f**,**g**) lenses of limestone, (**h**) coarse-grained sandstone, (**i**) lower contact of Kuldana Formation, (**j**) cyclic deposition of shales and sandstone, (**k**) sandstone lens in shales, (**l**) variegated colored pencil-like shales and limestone bed.
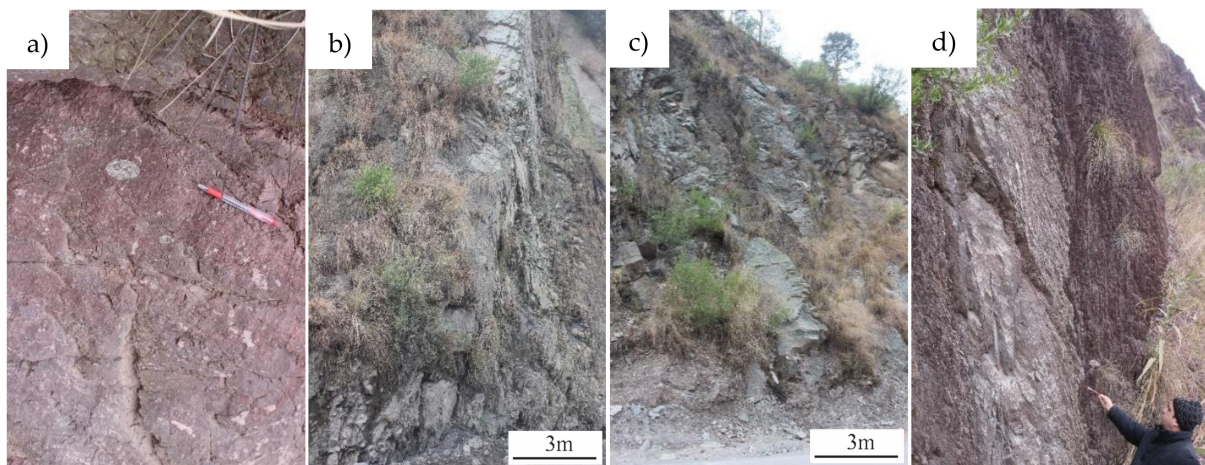
Figure 4. Photomicrograph showing (**a**,**b**) Dolomitic mudstone bed, (**c**) coarse-grained sandstone bed, and (**d**) erosional upper contact with the Murree Formation.
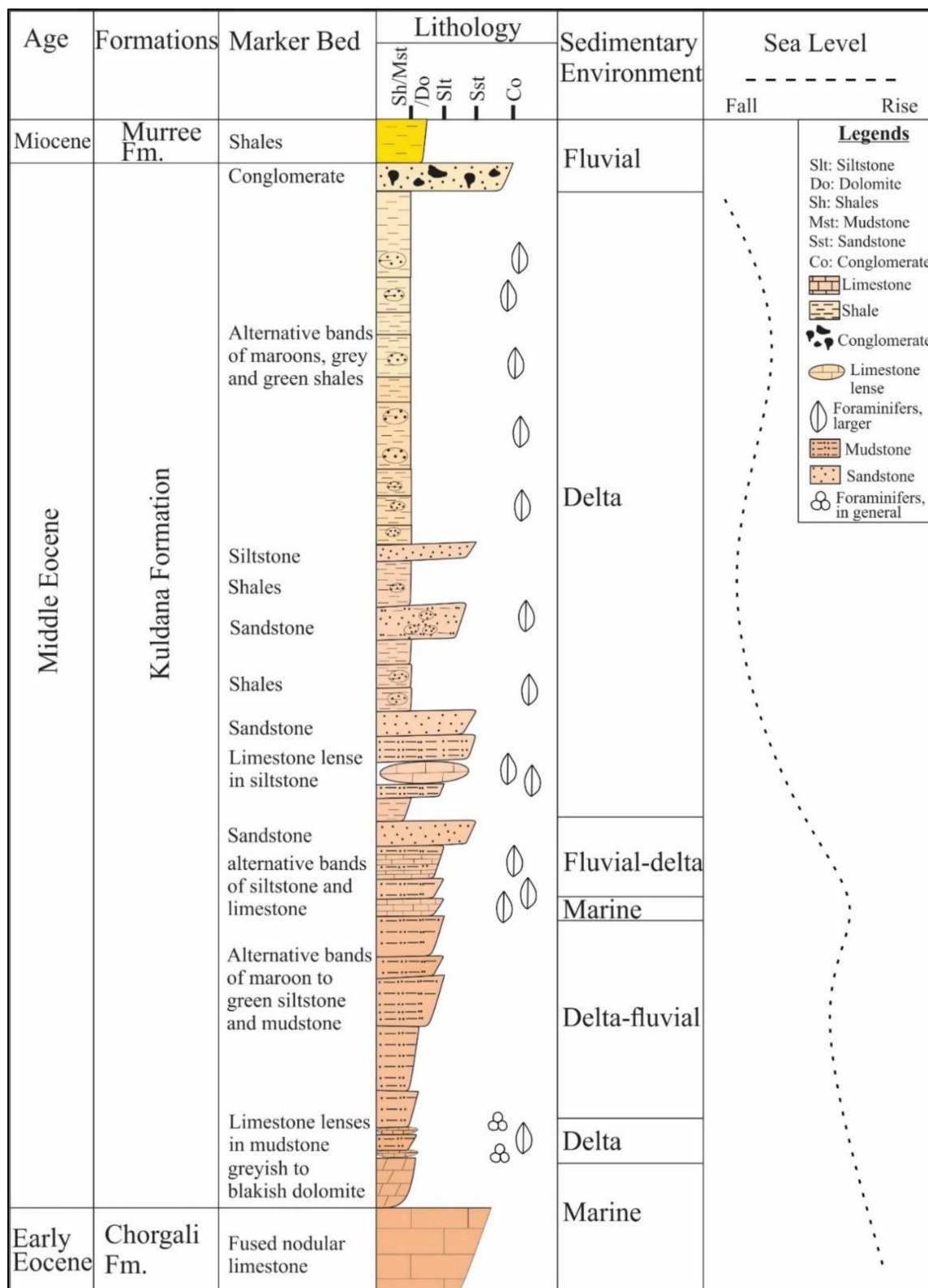
Figure 5. Log displaying the Yadgaar section lithology of the Kuldana Formation from the Muzaffarabad rea.

2. Materials and Methods

Two-week fieldwork of the Yadgaar Section was carried out (Figures 3 and 4). The Yadgaar section extends from Muzaffarabad city to Ghori village in Pakistan (Figure 1b).

Fieldwork includes identifying the formation and marking the top and bottom of the Kuldana Formation (Figure 5). Photographs of the field and outcrops were taken using a digital camera. The petrological investigation of the sandstone was used to deduce the climatic conditions, tectonic settings, and source types during the deposition of the Kuldana Formation. About twenty (20) representative fresh Kuldana Formation sandstone and limestone samples were collected from various locations for thin section preparation in the laboratory. A petrographic microscope was used for the thin section investigation (Leica DM-750P with an attached Leica EC3 camera, Leica Microsystems Ltd., Heerbrugg, Switzerland)). The Gazzi-Dickinson method was used to quantify sandstone components [44,45]. Aside from this, seven samples of fossiliferous limestone from the Kuldana Formation were also examined under a petrographic microscope. The texture and composition of limestone, such as the texture and composition of sandstone, reflect its depositional setting. The schemes of Dunham [46] and Folk [47] were used to classify the limestone of the Kuldana Formation.

3. Results and Discussion

3.1. Field Study

The Kuldana Formation is composed of mudstone (Figure 3a), variegated-colored shales (Figure 3b,c), lenses of limestone (Figure 3f,i), and sandstone (Figure 3e–h or Figure 4c). The shale colors are purple, red, green, maroon, crimson, pale grey, and brownish-grey. Cross-bedding, carbonate concretions, and reduction spots (spherical and elongated) (Figure 3d or Figure 4a) in shales were among the primary sedimentary features discovered in the field. Cross-cutting calcite veins were also seen in both sandstone and shale.

In certain locations, variegated-colored mudstones were extremely deformed and had been transformed into shales, with a pencil-like cleavage (columnar shales; Figure 3j–l). The Kuldana Formation coursing upward succession was transported by the river system and subsequently deposited in deltas. At the base, mudstone and shale were deposited, followed by sandstone (Figure 4c). This suggests a coarsening upward sequence transported by the river system and ultimately deposited in deltas.

3.2. Petrography of Sandstone Rocks

Using the method of Gazzi-Dickinson, the sandstone of the Kuldana Formation is classified is arenite. This is because each sample induced less than 15% matrix (Table 1). The ternary diagram of Folk [47] was used to determine the model values of quartz, rock fragments, and feldspar (Figure 6). Except for three samples, all of the samples are classified as litharenites (Figure 6a; Table 1). Using fragments of volcanic-plutonic, sedimentary, and metamorphic rock, litharenite and feldspathic litharenite are further subdivided. Twenty samples make up the phyllarenite, seven samples comprise the sedlithite, and a single sample was identified as volcanic arenite (Figure 6b). The Koldana Formation has two types of carbonate rocks: limestone and dolostone. According to the Folk [47] classification, the limestone is classified as biomicrite. In this formation, polycrystalline quartz decreases from base to top, whereas monocrystalline quartz progressively increases (Figure 7). Alkali feldspar, such as microcline and perthite are rarely found unevenly, while samples from the middle to the top are rich in orthoclase. Fragments of igneous rock are abundant at the base-middle and begin to decrease upwards. Fragments of metamorphic and sedimentary rock are abundant in the base and middle portion of the stratum and decrease towards the top. In terms of accessory minerals, hematite predominates in the middle portion of the formation, while muscovite, chlorite, rutile, tourmaline, and a few others are rare and unevenly distributed. There is a little increase in the percentage of calcite in the middle portion of the formation, although clay and chlorite are only identified in the top portion.

Table 1. Modal mineralogy of feldspathic litharenite and litharenites of Kuldana Formation. Moreover, displaying the end factors of quartzose parts of the sandstone was reevaluated for the diamond diagram of Pettijohn, et al. [48].

Sample No.			K-14	K-15	K-16a	K-16b	K-17	K-19	K-20	K-21	K-22	K-23	K-24	K-25	K-26	K-27	K-28	K-29a	K-29b	K-30	K-35	K-36
Quartz	Polycrystalline	2–3 grains	5	5	12	12	8	10	8	5	6	1	3	3	1	1	4	4	3	3	4	2
		>3 grains	3	5	6	8	9	8	7	3	3	5	5	8	5	3	6	3	5	2	5	3
	Monocrystalline	Qnu	17	15	8	9	10	6	10	5	5	20	15	15	26	24	25	20	20	25	24	25
		Qu	8	12	10	10	12	11	12	6	10	3	5	3	3	4	5	10	4	10	4	4
Feldspar	Plagioclase		3	-	2	2	-	1	1	-	2	1	-	-	2	2	-	2	3	-	-	-
	Perthite		-	-	1	-	-	-	-	-	-	-	-	-	-	-	-	-	-	-	1	-
	Microcline Perthite		2	1	-	-	1	-	1	1	-	-	-	-	2	-	-	1	-	-	-	1
	Orthoclase		1	4	-	2	1	1	4	1	3	1	2	5	-	1	4	1	4	2	2	1
Rock Fragments	Igneous	Rhyolite	6	4	2	2	4	2	3	3	1	2	-	5	-	1	-	5	1	1	2	3
		Basalt	1	-	1	1	1	1	1	2	3	4	7	2	2	2	4	2	2	-	1	-
	Metamorphic	Slates	5	2	2	5	6	8	8	-	-	5	2	3	8	3	5	6	-	2	-	5
		Schist	-	-	1	1	-	-	-	3	5	3	7	-	-	4	-	2	8	-	2	-
		Gneisses	-	-	1	-	-	1	-	-	-	-	-	2	-	-	-	-	-	-	-	-
		Quartzite	-	-	-	-	-	-	-	-	-	-	-	4	-	-	-	-	-	-	-	-
		Greenstone	-	-	-	-	-	-	-	3	-	-	-	-	-	-	-	-	-	-	-	-
	Sedimentary	Sandstone	3	3	5	5	3	4	6	5	7	5	2	3	5	8	-	5	2	7	5	-
		Siltstone	2	5	-	-	-	1	2	3	2	3	5	-	3	-	3	3	-	2	-	2
		Dolostone	-	5	-	-	2	-	-	-	-	-	-	5	-	-	-	-	-	-	-	-
		Limestone	-	6	18	7	7	6	7	15	12	13	-	-	-	-	-	-	-	-	-	7

Table 1. *Cont.*

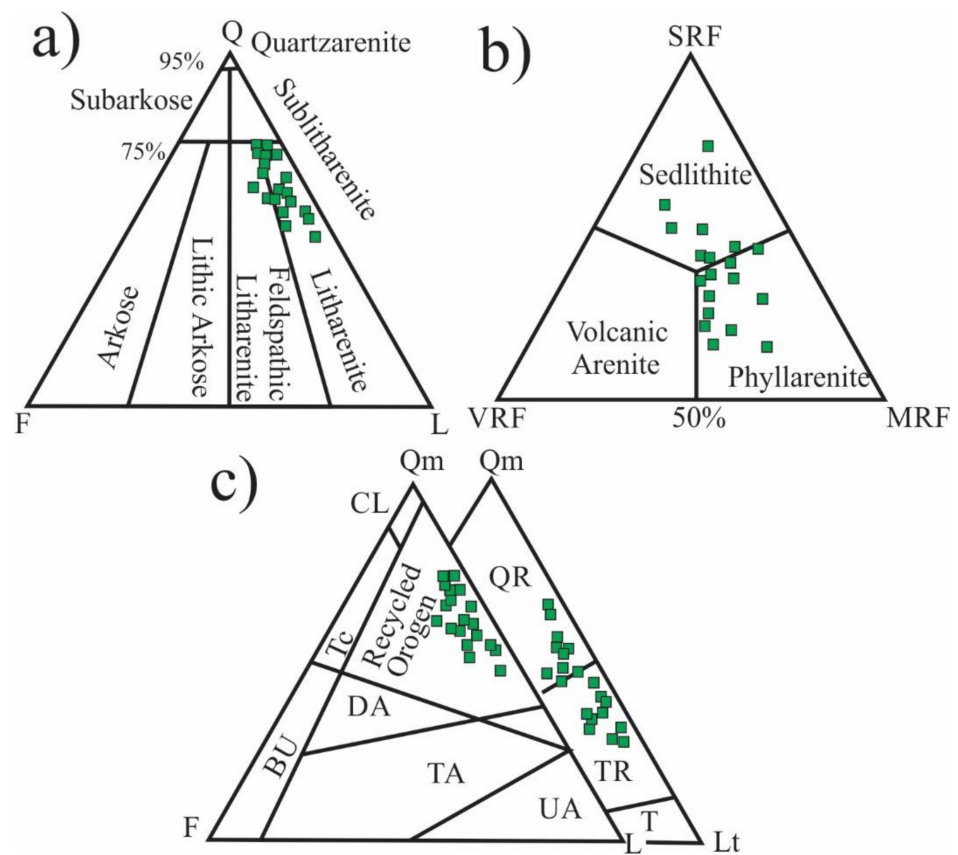| Sample No.		K-14	K-15	K-16a	K-16b	K-17	K-19	K-20	K-21	K-22	K-23	K-24	K-25	K-26	K-27	K-28	K-29a	K-29b	K-30	K-35	K-36
Accessory Minerals	Rutile	1	1	1	1	-	-	-	-	1	-	-	10	-	-	-	-	-	-	-	-
	Opaque	-	-	-	-	-	1	-	-	1	-	-	3	1	1	-	-	-	-	-	-
	Tourmaline	-	1	2	1	-	-	1	-	1	-	1	1	-	1	1	-	2	-	1	-
	Apatite	-	-	1	1	1	1	1	-	-	-	-	-	1	-	-	-	-	1	-	-
	Zircon	-	1	1	1	1	-	1	1	-	-	-	-	-	1	-	-	-	-	1	-
	Epidote	-	-	-	-	1	1	1	-	-	-	-	-	-	-	-	-	-	-	-	-
	Spinel	-	-	-	-	-	1	1	-	-	-	-	1	-	-	-	-	-	-	-	-
	Hematite	1	3	5	4	6	8	5	4	-	10	-	-	8	8	3	5	-	4	4	3
	Muscovite	-	-	3	1	1	1	1	1	1	1	2	-	-	-	1	3	1	1	-	-
	Biotite	-	-	1	-	-	1	-	-	-	-	-	-	-	-	-	-	-	-	3	2
	Chlorite	3	-	1	1	1	-	-	-	1	1	2	-	-	-	-	1	-	1	-	-
	Pumpellyite	1	-	-	-	-	-	-	-	-	-	-	-	-	-	-	-	-	-	-	-
	Sericite	1	-	1	-	-	-	-	-	-	-	-	-	-	-	-	-	-	-	-	-
	Prehnite	3	-	-	-	-	-	1	-	-	-	-	-	-	-	-	-	-	-	-	-
Cementing Material	Calcite	12	12	-	13	15	13	12	33	20	15	12	17	13	-	9	12	15	25	15	13
	Kaolinite Clay	-	-	-	-	-	-	-	-	-	-	-	2	-	10	11	-	8	-	8	5
	Hematite	5	6	-	10	10	11	6	3	6	-	12	-	8	13	9	8	7	6	9	6
	Dolomite	1	-	-	-	-	-	-	-	-	-	-	-	-	-	-	-	-	-	-	-
	Chlorite	-	-	3	-	-	-	-	-	5	-	-	-	-	-	-	1	3	-	-	6
Matrix	-	10	7	10	3	-	2	-	3	5	7	12	8	12	13	10	6	12	8	9	12
Calcite Veins	-	1	-	2	-	-	-	-	-	-	-	-	6	-	-	-	-	-	-	-	-
Calcite Concretions	-	5	2	-	-	-	-	-	-	-	-	-	-	-	-	-	-	-	-	-	-
Total	-	100	100	100	100	100	100	100	100	100	100	100	100	100	100	100	100	100	100	100	100

Figure 6. (**a**,**b**) Modal mineralogy of the Kuldana sandstones on the Aurbach, et al. [49] diagram; (**c**) displaying triangular plot values (QtFL and QmFLt) for the provenance inter- pretation of samples from the Kuldana Formation (Lr, Lithic Recycling; Ci, Craton Interior; Tr, Transitional Recycling; Tc, Transitional Continent; Qr, Quartzose Recycling; Bu, Base-Ment Uplift; Ua, Undissected Arc; Ta, Transitional Arc; Da, Dissected Arc).
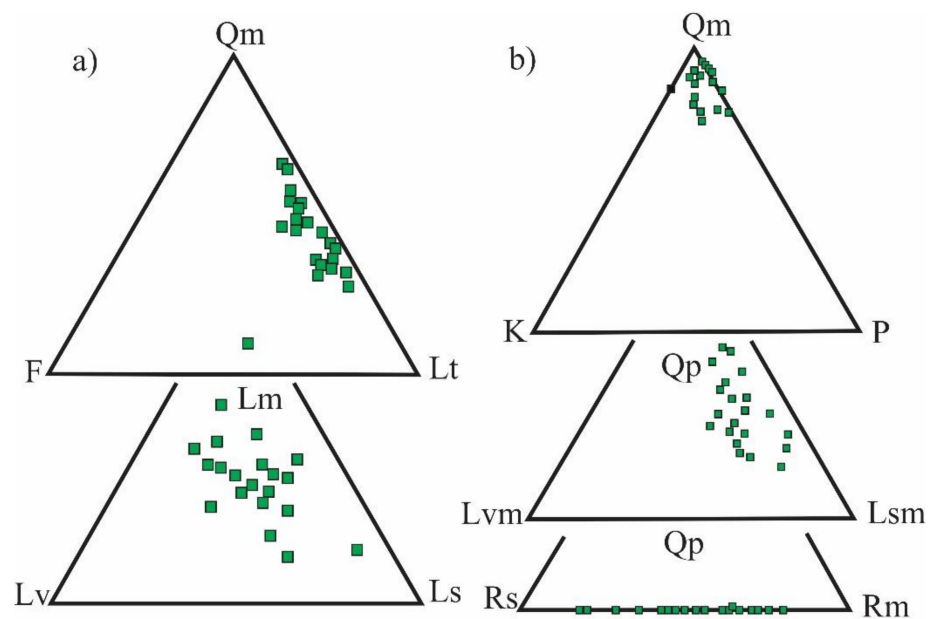

Figure 7. (**a**,**b**) QmFLt, QmPK, LmLvLs, QpLvmLsm, RgRsRm and ternary plots of sandstone samples.

3.2.1. Litharenite

Litharenites are medium-massive-bedded, greenish-dark gray, generally fine-coarse-grained, and relatively well-cemented sandstones. Quartz grains range between 19 and 40%, rock fragments between 10 and 23%, and feldspar between 2 and 5%. The matrix ranges from 2 to 13%. In the litharenite of the Kuldana Formation, both subrounded and angular quartz grains are observed (Figure 8a,b). There are fewer polycrystalline quartz grains (Qp) than monocrystalline quartz grains (Qm) (Figure 8a).
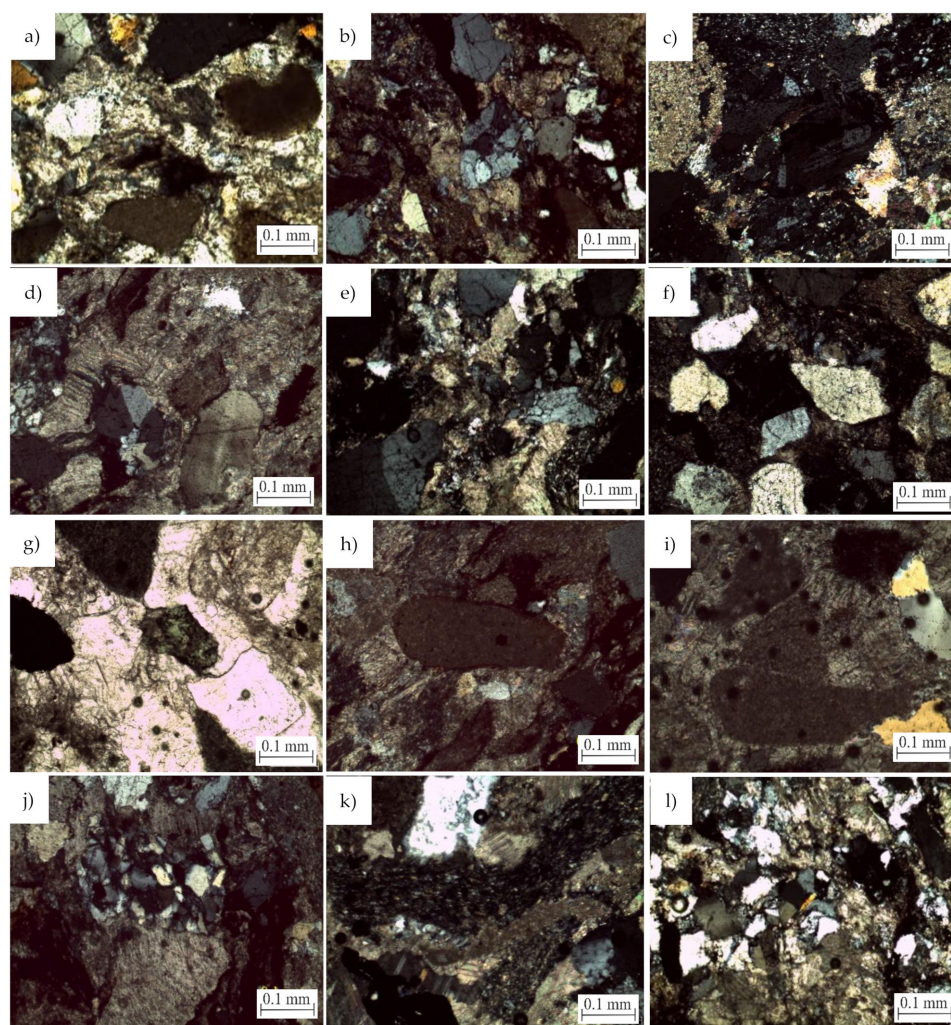
Figure 8. Photomicrograph illustrating (**a–c**) monocrystalline quartz, polycrystalline quartz and plagioclase, (**d**) orthoclase, (**e**) slate clast, (**f**) schist clast, (**g**) greenstone, (**h,i**) micritic limestone with pyrite and micritic limestone, (**j**) sandstone clast, (**k**) siltstone clast, and (**l**) tourmaline.

Feldspar varies between 2 and 5%. Plagioclase and alkali feldspar are the components of litharenite. Plagioclase (Figure 8c) grains have been altered into sericite. Perthite and orthoclase make up alkali feldspar (Figure 8d).

The percentage of rock fragments varies between 10 and 23%. The litharenite clast was comprised of sedimentary, metamorphic (Figure 8e), and igneous rocks, such as greenstone (Figure 8g), slate-schist (Figure 8f), volcanic (basalt) with plagioclase phenocrysts, granite, fine-grained gneisses, quartzite, limestone (Figure 8h), and rock fragments. Limestone clasts are micritic (Figure 8i). The litharenite has the highest proportion of low-grade metamorphic (slate) and sedimentary rock fragments of any rock. There were clasts of sandstone and siltstone in the litharenite sediment (Figure 8j,k). Slate clasts have also been seen in the litharenite.

The accessory minerals of litharenite include tourmaline (Figure 8l), apatite, epidote, spinel, hematite (Figure 9a,b), rutile (Figure 9c), biotite (Figure 9d), zircon (Figure 9e), and quartz (Figure 9f).
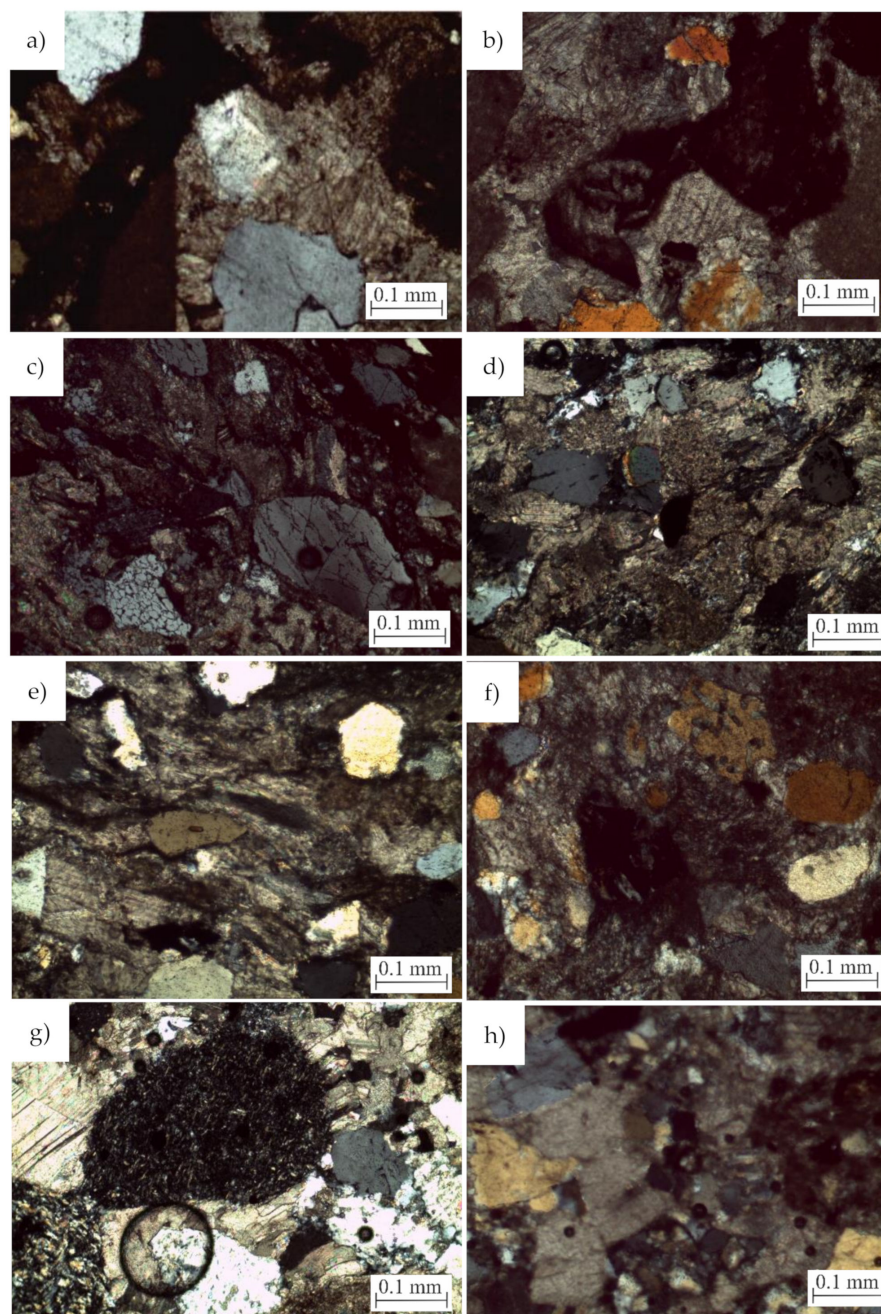

Figure 9. Photomicrograph showing (**a,b**) hematite, (**c**) rutile, (**d**) biotite, (**e**) zircon, (**f**) fluid inclusion in quartz, (**g**) volcanic clast, and (**h**) hematite clast in the litharenite.

The matrix ranges from 2–13%. Calcite (Figure 8c,g–i), hematite (Figure 8a,b,f,h, or Figure 9h), kaolinite clay, dolomite, and chlorite are common types of cement. The sub-categories of litharenite are sedlithite and phyllarenite.

3.2.2. Phyllarenite

Phyllarenite has been identified in 10 litharenite samples (K16b, K17, K19, K23, K24, K25, K26, K28, K29a, and K36). Quartz accounts for 24–40% of phyllarenite, rock fragments for 10–23%, and feldspar for 2–5%. The matrix ranges between 2 and 12% (Table 1).

3.2.3. Sedlithite

Sedlithite has been identified in seven litharenite samples as K15, K16a, K21, K22, K27, K30 and K35. In sedlithite, the quart, rock fragments, and feldspar are19–40%, 10–19%, and 2–5% respectively. Matrix ranging from 3–13% (Table 1).

3.3. *Feldspathic Litharenite*

Feldspathic litharenites are characterized by thick green-maroon sandstone layers. The grain size varies from fine to coarse. These strata of sandstone contained lenses of limestone as well. Hematite, calcite, kaolinite, and chlorite are sandstone cementing materials (Figure 9a–d,g). Q comprises 32–37% of feldspathic litharenites, rock fragments 13–20%, and feldspar 6–7%. The matrix varies by up to 12% (Table 1).

The Kuldana Formation litharenite is composed of sub-rounded, angular-sub angular, and quartz grains. In general, these grains are divided into three groups: non-undulating monocrystalline quartz, undulating monocrystalline quartz (Figure 10a), and polycrystalline quartz (Figure 10b).
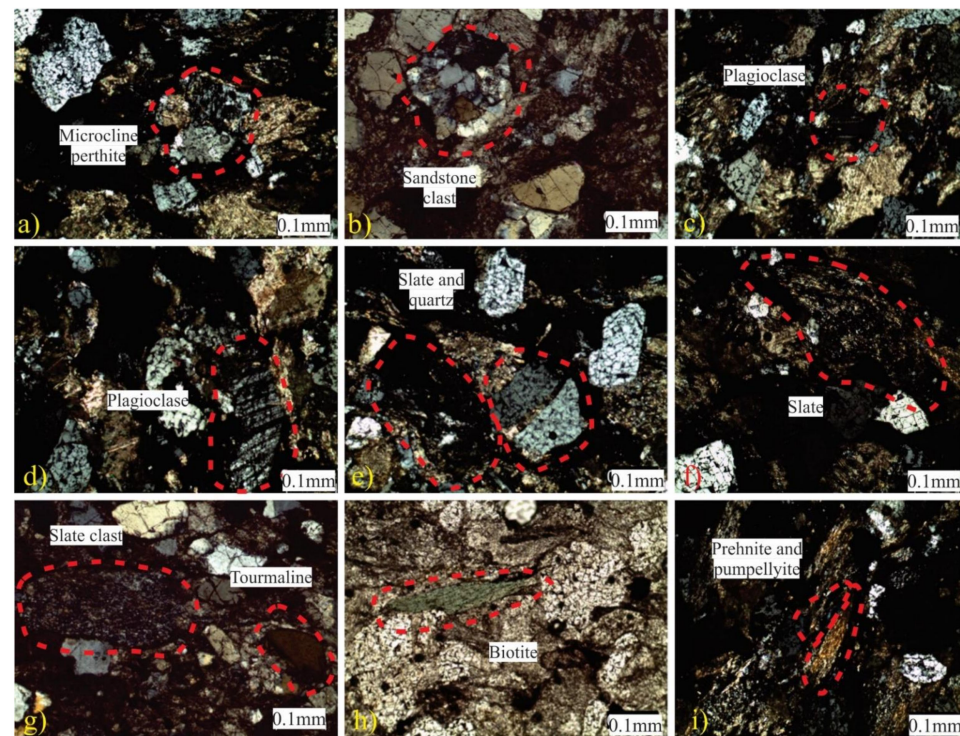
Figure 10. Photomicrograph displays (**a**–**c**) monocrystalline quartz in feldspathic litharinte, polycrystalline quartz and plagioclase, (**d**) microcline perthite, (**e**) slate, (**f**) sandstone, prehnite and pumpellyite in feldspathic litharenite, (**g**) tourmaline in feldspathic litharenite, (**h**) biotite in feldspathic litharenite and (**i**) prehnite and pumpellyite in feldspathic litharenite.

Due to metamorphism, quartz grains have a stretched and strained quality, which is shown by the relatively small amount of monocrystalline quartz. Contact between quartz grains is observed to be planar and concavo-convex. In the feldspathic litharenite, alkali feldspar, and plagioclase are the predominant types of feldspar (Figure 10c). Alkali feldspar comprises microcline perthite (Figure 10d), while feldspathic litharenite consists of igneous, metamorphic, and sedimentary rocks as clast (such as slate and sandstone; Figure 10e,f).

Tourmaline (Figure 10g), biotite (Figure 10h), pumpellyite, and prehnite (Figure 10i) were determined to be the predominant accessory minerals. Muscovite is formed from biotite by the processes of diagenesis or weathering in feldspathic litharenite. Feldspar, schist, and slate are influenced and transformed during diagenesis, resulting in the development of feldspathic litharenite. In feldspathic litharenite, many cementing elements

are present, including calcite (Figure 10c,d), kaolinite clay, hematite (Figure 10b,g), and dolomite. Further classifications for litharenites include volcanic arenites and phyllaries.

3.3.1. Phyllarenite

Two feldspathic litharenite samples are distinguished from phyllinite (K29b and K20). The proportion of quartz ranges from 32 to 37%, the proportion of rock fragments from 13 to 20%, and the percentage of feldspar from 6 to 7%. 0 to 12% is the percentage range for matrices (Table 1).

3.3.2. Volcanic Arenite

One sample is classified as volcanic arenite (K14). The basic mineralogy of this sample was comprised of 33% quartz, 17% rock fragment, % feldspar, and % matrix (Table 1).

3.4. Sandstone Composition of the Kuldana Formation

The modal mineralogical composition of the Kuldana Formation sandstone reveals a clear trend from base to top. It was noticed that the proportion of polycrystalline quartz and volcanic, sedimentary, and metamorphic rock fragments decreased gradually. In contrast, a rise in monocrystalline quartz and orthoclase has been noticed in the sandstone of Kuldana Formation. The detrital components observed in the sandstone of Kuldana Formation suggest compositional diversity, hence explaining its source type.

The compositional mean of the all samples is Qm36 F24 Lt40, which is composed of quartzose-lithic in composition (Table 2). Lithic fragments range from 27–51% (Qm-FLt%Lt), monocrystalline quartz from 19–55% (QmFLt%Qm), and feldspar from 18–33% (QmFLt%F) (Figure 7a). Alkali feldspar is somewhat more abundant than plagioclase feldspar (Qm36 $\pm$ 6 P4 $\pm$ 2 K9 $\pm$ 3; Tables 2 and 3).

Lithic fragments (aphanitic) (Lm37 $\pm$ 6 Ls37 $\pm$ 6 Lv26 $\pm$ 5; Table 2) consists mostly of metasedimentary (slate, schist, quartzite, greenstone, and gneiss) and sedimentary grains (sandstone, siltstone and carbonate rocks) (Table 3). Furthermore, there were fewer basaltic and rhyolitic volcanic clasts than metasedimentary/sedimentary clasts (Figure 9g).

In the sandstone, metasedimentary/sedimentary clasts are more common than polycrystalline-quartz and meta-volcanic/volcanic fragments (Lsm46 $\pm$ 7 Lvm16 $\pm$ 4 Qp37 $\pm$ 6; Table 2; Figure 7b). In addition, fine-grained plutonic clasts were almost absent. On the other hand, metasedimentary clasts and sedimentary clasts were observed in equal proportion (Rm49 $\pm$ 7 Rs51 $\pm$ 7 Rg0 $\pm$ 0; Figure 9e–g; Table 2).

Interpretation

Recycled orogenic provenance was suggested for the Kuldana sandstone by analyzing QtFL and QmFLt ternary diagrams and the recycled orogenic origin of transitional-quartzose (QmFLt plot; Figure 6c). Stratified rocks may be recycled through tectonic uplift, deformation, and erosion [20]. Due to the Himalayan Orogeny, the Kuldana Formation was deposited in the Foreland Basin. The mineral composition of the sandstone reflected the geological setting of the area. Non-undulatory quartz grains originate from granite, but undulatory quartz grains may be derived from high-grade metamorphic rocks [10]. Basaltic clasts of volcanic rocks are likely associated with the Panjal Formation (Permian) or other basaltic Himalayan rocks [50]. The Panjal Formation consists of carbonates and basaltic lava flows. The presence of heavy minerals in clastic sedimentary rocks is noteworthy due to the fact that these minerals serve as provenance markers [51]. Most reworked sediments have subrounded or rounded grains [52]. Zircon grains in the sandstone of the Kuldana Formation are rounded to sub-rounded, suggesting that they originated from igneous and metamorphic processes. The tourmaline family of minerals exhibits a vast spectrum of colors and chemical compositions. Due to their diverse chemical components, they all display pleo-chroism [53]. The formation contains subrounded grains of dravite that are yellow-brown. The occurrence of epidote in Kuldana Formation sandstone may have originated from metamorphic rocks, such as green-schist facies.

Table 2. Recalculated detritus of Kuldana sandstone.

S#	QtFL%			QmFLt%			QmPK%			LmLvLs%			QpLvmLsm%			RgRmRs%		
	Qt	F	L	Qm	F	Lt	Qm	P	K	Lm	Lv	Ls	Qp	Lvm	Lsm	Rs	Rm	Rg
K-14	58.9	10.7	30.3	37.3	25.3	37.3	80.6	9.6	9.6	29.4	41.1	29.4	32	28	40	50	50	0
K-15	66	8.9	25	41.5	21.5	36.9	84.3	0	15.6	14.2	28.5	57.1	41.6	16.6	41.6	20	80	0
K-16a	70.5	5.8	23.5	30	20	50	85.7	14.2	0	33.3	25	41.6	60	10	30	44.4	55.5	0
K-16b	68.4	7	24.5	28.3	20.9	50.7	82.6	8.6	8.6	42.8	21.4	35.7	58.8	8.8	32.3	54.5	45.4	0
K-17	70.9	3.6	25.4	32.8	20.9	46.2	91.6	0	8.3	42.8	35.7	21.4	54.8	16.1	29	66.6	33.3	0
K-19	64.8	3.7	31.4	24.6	24.6	50.7	89.4	5.2	5.2	52.9	17.6	29.4	51.4	8.5	40	64.2	35.7	0
K-20	58.7	9.5	31.7	28.5	25.9	45.4	78.5	3.5	17.8	40	20	40	42.8	11.4	45.7	50	50	0
k-21	47.5	5	47.5	19.3	33.3	47.3	84.6	0	15.3	31.5	26.3	42.1	29.6	18.5	51.8	42.8	57.1	0
K-22	51	10.6	38.2	25	30	45	75	10	15	27.7	22.2	50	30	23.3	46.6	35.7	64.2	0
K-23	54.7	3.7	41.5	31.5	30.1	38.3	92	4	4	36.3	27.2	36.3	21.4	21.4	57.1	50	50	0
K-24	52.8	3.7	43.3	27	31	41.8	90.9	0	9.1	39.1	30.4	30.4	25.8	22.5	51.6	56.25	43.75	0
K-25	54.7	9.4	35.8	26.8	28.3	44.7	78.2	0	21.7	47.3	36.8	15.7	36.6	23.3	40	75	25	0
K-26	61.4	7	31.5	40.8	25.3	33.8	87.8	6	6	44.4	11.1	44.4	25	8.3	66.6	50	50	0
K-27	60.3	5.6	33.9	41.1	26.4	32.3	90.3	6.4	3.2	38.8	16.6	44.4	18.1	13.6	68.1	46.6	53.3	0
K-28	71.4	7.1	21.4	46.8	18.7	34.3	88.2	0	11.7	41.6	33.3	25	45.4	18.1	36.3	62.5	37.5	0
k-29a	57.8	6.2	35.9	36.1	27.7	36.1	88.2	5.8	5.8	34.7	30.4	34.7	23.3	23.3	53.3	50	50	0
K-29b	61.5	13.4	25	41.3	22.4	36.2	77.4	9.6	12.9	61.5	23	15.3	38.1	14.2	47.6	80	20	0
K-30	74	3.7	22.2	54.6	18.7	26.5	94.5	0	5.4	16.6	8.3	75	29.4	5.8	64.7	18.1	81.8	0
K-35	74	6	20	49.1	17.5	33.3	90.3	3.2	6.4	20	30	50	47.3	15.7	36.8	28.5	71.4	0
K-36	73.9	4.3	21.7	53.7	18.5	27.7	93.5	0	6.4	50	30	20	33.3	20	46.6	71.4	28.5	0
Means	62.6	6.7	30.5	35.8	24.3	39.7	86.2	4.3	9.4	37.2	25.7	36.9	37.2	16.4	46.3	50.8	49.1	
Standard Deviation	7.9	2.6	5.5	5.9	4.9	6.3	9.2	2	3	6.1	5	6	6.1	4	6.8	7.1	7	0

Table 3. Kuldana Formation evaluation, based on the following petrographic and other key parameters.

S. No	
1.	**Quartzose Grains (Qt = Q = Qm + Qp) Qt = total quartzose grains**
	Qm = monocrystalline quartz (Qm = Qu + Qnu)
	Qu = Undulatory monocrystalline quartz
	Qnu = Non undulatory monocrystalline quartz
	Qp = polycrystalline quartz (Qp = Qp2–3 + Qp > 3) Qp2–3 = Polycrystalline quartz, 2–3 grains
	Qp > 3 = Polycrystalline quartz, more than 3 grains
2.	**Feldspar Grains (F = P + K)**
	F = Total feldspar grains P = Plagioclase feldspar K = Potassium feldspar
3.	**Unstable lithic Fragments (L = Lsm + Lvm) L = total unstable lithic fragments**
	Lsm = total sedimentary and metasedimentary fragments (Lsm = Ls + Lm)
	Ls = sedimentary lithic fragments
	Lm = metasedimentary lithic fragments
	Lvm = total volcanic and metavolcanic lithic fragments
	Lv = total volcanic lithic fragments
	VRF = volcanic-plutonic rock fragments
	SRF = sedimentary rock fragments including extrabasinal detrital limeclasts
	MRF = metamorphic rock fragments
4.	**Total Lithic Fragments (Lt = L + Qp)**

Rutile grains have a sub-rounded shape, indicating that they are likely to have originated from reworked sediments. According to Bossart [54], the presence of sericite, chlorite, and pumpellyite in the reed beds of the Balakot Formation indicates pumpellyite-grade metamorphism. Thin sections of the Yadgaar Section also exhibit the presence of pumpellyite, sericite, and chlorite, which clearly indicates prehnite-pumpellyite metamorphism. Zircon, rutile, and apatite all indicate an igneous and metamorphic origin [55]. In thin sections, tourmaline, quartz, and a small quantity of feldspar can also be observed. The origins of tourmaline are pegmatites, schists, and granites [56]. Quartz and feldspar indicate an orogenic origin from which these minerals and the large river sediments reached the foreland basins [57]. In general, the characteristic quartz lithic petrofacies show that the source type and paleoclimatic environment were almost constant throughout the deposition of Kuldana Formation sandstones.

3.5. Petrography of Carbonate Rocks

The carbonate rocks of the Kuldana Formation are classified into dolostone and limestone. The limestone is characterized as biomicrite by using Folk [47] classification. However, based on the textural classification of limestone, the limestone of the Kuldana Formation is distinguished as mudstone, wackestone, and packstone. The bioclasts include *Nummulites atacicus*, *Nummulites mamillatus*, *crinoids*, *Nummulites discorbina*, *Nummulites djodjokartae*, *Nummulites vascus*, *Lockhartia pustulosa*, gastropods, miliolids, brachiopods, *Globigerinoides* spp., bivalves and ostracodes suggesting a Middle Eocene to Oligocene age for the Kuldana Formation (Figure 11). The diagenetic features including micro-fractures, pressure solution and stylolites of low and high amplitude can also be observed. The mudstone contributes 1–5 m thickness (Figure 4).
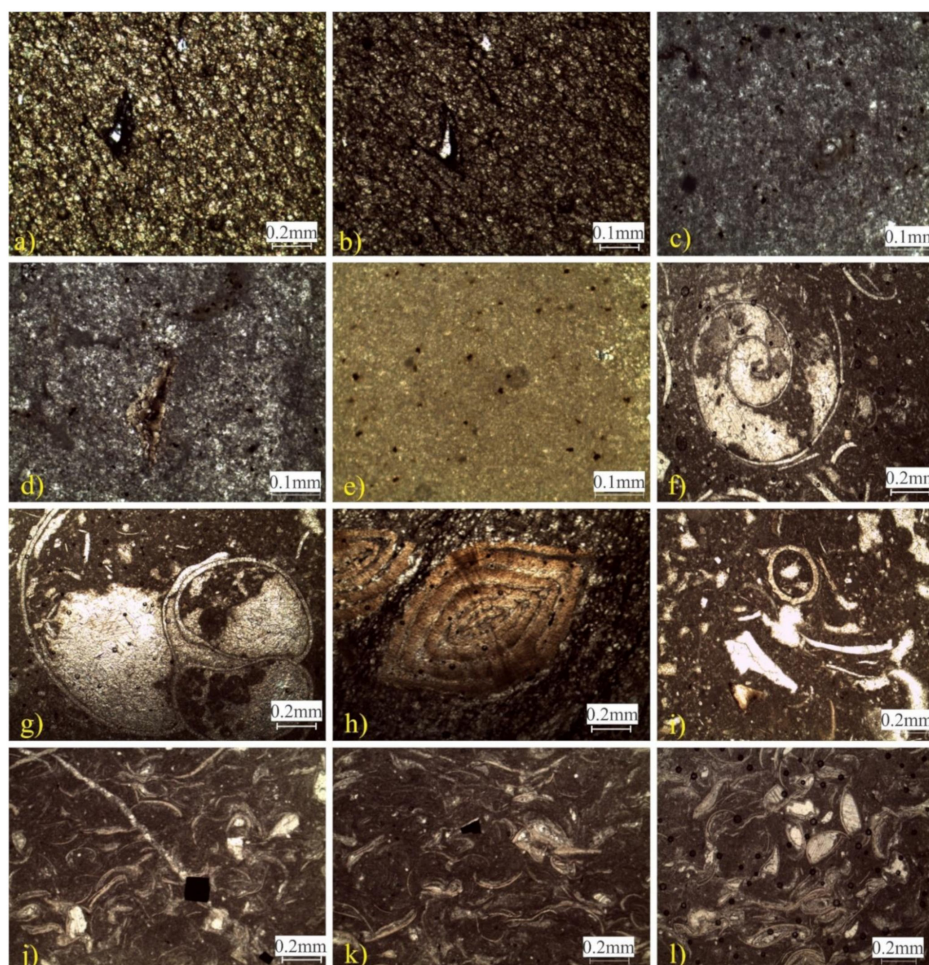
Figure 11. Photomicrographs of the limestone of the study area: (**a**,**b**) Micritic mudstone with miliolids, (**c**,**d**) Chalcedony in micritic mudstone, (**e**) micritic mudstone, (**f**,**g**) Gastropods filled with spar, (**h**) *Nummulites* spp. in wackstone, (**i**) and bioclast (**j**–**l**) Ostracods filled with spar, Pyrite and Calcite vein.

3.5.1. Mudstone

Mudstone petrofacie's ranges in thickness from 2 to 6 m and accounts for 8% of the total volume of rock (Figure 11a–e). Micrite (90–95%), bioclasts (1–3%), pyrite (2–6%), chalcedony (0–1%), and chert and quartz are observed in two samples (K1 and K2). The predominant constituents of mudstone petrofacies are micrite matrix and partially dolomitized patches. The identified fossils include *Pyramidellidae gastropoda* (Figure 10f,g) and miliolids (Figure 11a,b). Chert is also visible in thin sections. Diagenetic characteristics such as micro-fractures, pressure solution, and low and high amplitude stylolites may also be detected.

Interpretation

The presence of *pyramidellidae* gastropoda in the dolomitized mudstone-dominated lithology indicates deposition occurred in a low-energy shallow-water lagoonal environment [24–29]. The majority of current observations of this species originate in shelf environments [24–29].

The dolomitization of sediments suggests fluid circulation [58]. The dolomitization verifies the lagoonal environment with shallow water [24–29,57–61]. Pyrite (an authigenic mineral) represents typical marine and freshwater ecosystems. This demonstrates a restricted lagoonal environment. Therefore, a high concentration of scattered pyrite is a

prevalent precipitate in sediments that underwent diagenesis in an alkaline and reducing environment [62].

Miliolids and an abundance of micrite matrix are indicative of shallow water lagoonal platform environments [63]. A high proportion of micrite suggests that wave energy or current was insufficient to dissolve the fine matrix in a specific area [64,65]. Mudstone facies are deposited in an environment with low energy, either in protected seas or beneath a fair-weather base (calm water) [66].

The considerable quantity of mud matrix in the sediments suggests a slow rate of sedimentation [67]. As with benthic foraminifera, micritic facies suggests a relatively shallow marine environment [65]. In a few instances, the back reef or lagoon is an ideal environment for micritization [68]. The deposition of micrites may be considerably facilitated by a calm and low-energy water environment [69]. Silicification may be triggered at any stage of digenesis, from early to late. The presence of chert in the lower portion of the Kuldana Formation's limestone also implies a shallow marine environment with a terrestrial input source (river water with a high silica concentration) (Figure 11). Laschet [70] shown that "terrestrial" is the most important source of silica in shallow marine environments. This petrofacies is deposited in the surroundings of the inner ramp to the outer ramp.

3.5.2. Wackstone

Micrite makes up the majority of wackstone. A carbonate rock that is mud-supported and contains >10% grains is called wackstone. Three wackstone samples, K3, K23, and K34, are composed mostly of micrite (40–60%), bioclasts (15–25%), spar (0–15%), organic (0–10%), terrigenous (0–35%). The limestone is called biomicrite because it is composed of bioclasts deposited in a micrite matrix. Figure 10i or Figure 11h depict bioclasts identified as gastropods, *Nummulites*, and *Lockhartia* spp.

Interpretation

The presence of gastropods indicates that limestone was deposited in shallow, low-energy marine or lagoonal environments [71–74]. The occurrence of *Nummulites* indicates a quick deposition of silt on the middle ramp (Figure 11h–l) [75–77]. *Lockhartia* spp. similarly indicate the inner-middle ramp depositional area [78].

A low proportion of bivalves and *Nummulites* among the gastropods indicates that deposition occurred in the deeper portion of the marine shelf and at the lagoon's edge [79]. There is an abundance of benthic foraminifera in shallow marine environments.

The presence of fragmented skeletal remains suggests that the depositional environment may have been somewhat disturbed. The association of gastropods and bivalves suggests brackish, lagoonal facies. One of the most distinguishing features of the lagoon is that almost all gastropod shells are filled with thin cement [80]. The abundance of nummulites and associated foraminifera indicated deposition in an open sea or inner-ramp environment [81]. Detrital monocrystalline quartz grains indicate a slope environment. According to Dunham [46], wackstone is a carbonate rock with a mud-supported structure and low hydraulic energy of deposition.

3.5.3. Packstone

The term "packstone" refers to a carbonate rock that is mostly composed of micrite and contains at least 1% of mud-grade fragments. Two packstone samples (K4 and K13) are dominated by micrite (45–48%) and bioclasts (45–48%), but calcite (0–2%) and pyrite (0–2%) are also observed. The limestone is referred to as biomicrite because it is composed of bioclasts deposited within a micrite matrix. The presence of ostracods, bivalved brachiopods (Figure 11k,l), Globgerinoides (Figure 12a–g), Nummulites (Figure 12h–j,m) and Lockhartias species has been reported as well (Figure 12n,o).

Figure 12. Photomicrographs of the bioclasts found in the limestone of the study area. (**a–g**) *Gloibigerinoides* species, *nummulites* spp. (**h–j,m**), ostracods and bivalved brachiopods (**k,l**), *Lockhartias* spp. (**n,o**).

Interpretation

This petrofacie consists of ostracods that evolved between the Late Paleozoic and the Cenozoic [82]. Ostracods inhabit a variety of environments, including marine, transitional, and even freshwater. They are widespread from the equator to the polar seas and are found at different depths ranging from the shoreline to the bathyal zone [76]. Initially, brachiopods are inhibited at moderate water depths, usually above seamounts. Occasionally, they are transported as bypass margins from their original place to the slope angle under the influence of gravity. They eventually settled at the base of seamounts. The habitats of bivalves are diverse, ranging from nearshore to offshore conditions and even to shoral environments [83]. The features of these microfacies reveal that deposition occurs under conditions of slightly higher energy (Figure 12).

3.6. Tectonic Settings and Provenance

In the middle-late Eocene, detrital sedimentary influx supplied the Himalayan Foreland basin of Indo-Pakistan with a cover sequence dominated by sandstone, siltstone, limestone, and shale facies. In the Indian areas of Jammu and Himachal Pradesh, these

deposits are located in the middle-upper Subathu Formation. The Middle-upper Subathu Formation is further subdivided into Kalakot member/zone II–V (middle Eocene) and Arnas member/zone VI–V (late Eocene) (middle Eocene-early Miocene). The Kuldana Formation is stratigraphically comparable to the lower-middle Subathu Formation in the Kohat, Hazara, and Kashmir regions (Figure 2) [84]. Typically, members of the late Kalakot Formation and the early Arnas Formation are identical to those of the Kuldana Formation.

In accordance with Dickinson [85], ternary diagrams of QtFL and QmFLt are used for provenance analysis. The QtFL diagram is filled with plots having recycled orogens as their origins. It suggests that transitional-quartzose recycled orogenic material is the source of recycled quartzose orogenic material (Figure 13). The sandstone contains fragments of igneous, metamorphic, and sedimentary rocks, among many others.
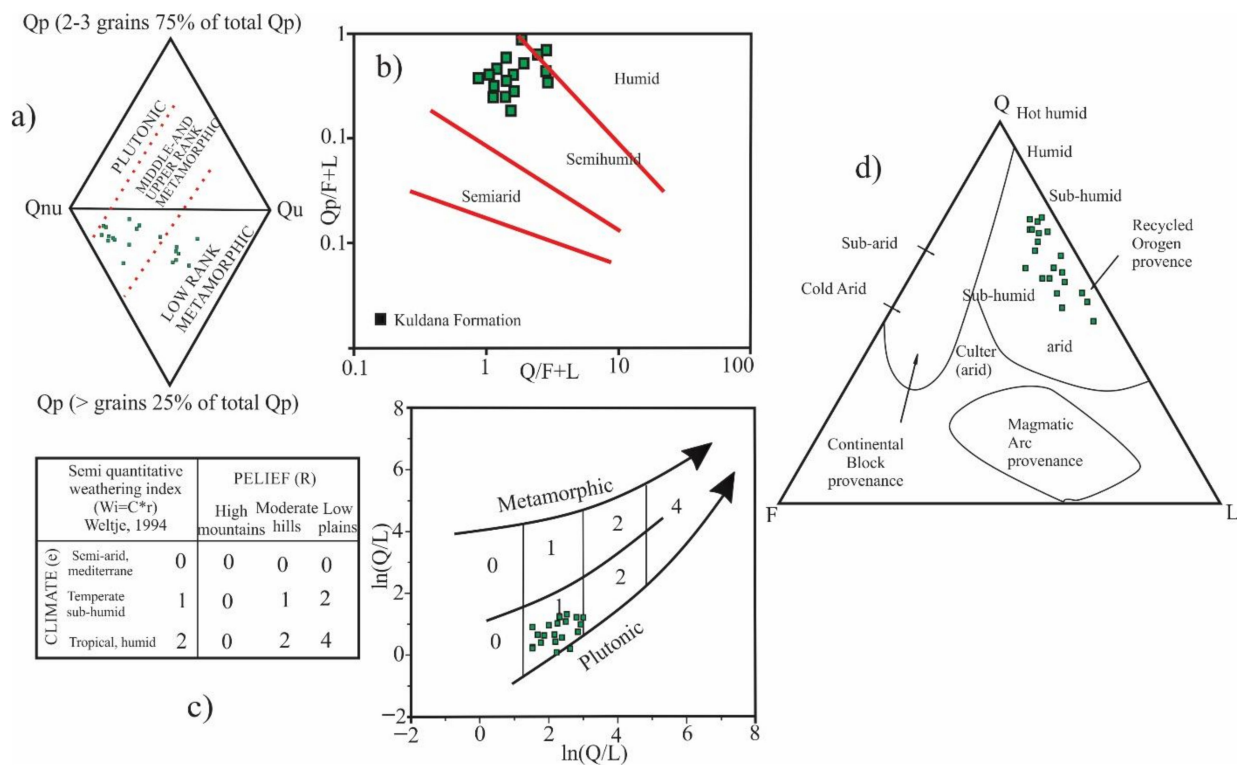
Figure 13. (**a**) A diamond diagram is shown for the interpretation of the Kuldana Formation's provenance, (**b**) based on the Suttner and Dutta [86], plot of sandstone samples on the Q/(F + RF) vs. Qp/(F + RF), interpretation of the paleo-climatic conditions, (**c**) semi-quantitative weathering index and weathering diagram, (**d**) adapted from Suttner and Dutta [86], interpretation of ternary diagrams for sandstones in the Kuldana Formation (based on QFL ternary diagrams).

Previous researchers identified the fragments of volcanic rock from the upper Subathu Formation in the Shimla Hills indicate an ophiolitic origin.

Previous research determined that volcanic rock fragments from the upper Subathu Formation in the Shimla Hills are of ophiolitic origin. The presence of volcanic and metamorphic clasts in the Subathu Formation, Kasauli Formation, Dagshai Formation, and Balakot Formation in the HFB indicated a recycled orogenic provenance [87]. They proposed an arc-type ophiolite genesis for these formations. They also argued that ophiolitic and metamorphic detritus may have been recycled from the Indus Suture Zone and Himalayan thrust sheets from the north, indicating the closing of the Ceno-Tethys Ocean. Previous studies on the sedimentary sequence of the passive continental margins revealed the presence of volcanic, metamorphic, and metasedimentary detritus, indicating a rapid rate of sedimentary accumulation induced by a recycled orogeny and also indicating the Ceno-Tethys Ocean closing event [13].

However, the present study revealed the presence of metamorphic and (basaltic) volcanic clasts in the sandstone of the Kuldana formation that were derived from the Lesser and Higher Himalayas (Figure 9g). While sedimentary rock fragments (sandstone, slate, and carbonate clasts) were derived from the Cambrian-Eocene in age, they derive from the Tethyan succession. Throughout the Himalayas, sedimentary and low-grade metamorphosed rocks of the Cambrian-Eocene Tethyan succession are exposed [16].

By using the modal data in a diamond diagram of Basu [35], the sediment source and tectonic setting have been determined (Figure 13a; Table 1). All sandstone samples had a mean of Qnu66.4 Qu23.4 Qp > 310.1. In sandstone, non-undulatory monocrystalline quartz (Qnu) is more prevalent than undulatory and polycrystalline quartz (Qp). Sandstone seems to include a greater proportion of monocrystalline quartz (Qnu) with non-undulating surfaces than monocrystalline (Qu) and polycrystalline (Pc) (Qp).

Qnu is more abundant in the Kuldana Formation, suggesting that plutonic activity was the source of the sandstone (granite) (Figure 13c). According to Basu [35], Qp and grain size have a strong correlation. Twenty sandstone samples from the Kuldana Formation seem to have provenances of mid-to-upper rank metamorphic layers, while seven samples have provenances of low-rank metamorphic strata, as shown by the results of the current study (Figure 13a). The Himalayas are the source of plutonic and metamorphic rocks based on these sediments.

In the northwest Himalayas, the lower Subathu Formation consists of interbedded shale and siltstone with angular quartz, muscovite, and carbonate-ferruginous cementing material. The lower portion of the Subathu Formation may consist of reworked carbonates, whereas the percentage of limestone intercalations increases upwards [78]. In Kashmir, the Yadgaar section of the Upper Indus Basin is composed of litharenite and feldspathic litharenite sandstones, suggesting a re-cycled orogenic origin and semiarid-semihumid environments (Figure 13b).

The presence of metamorphic clasts, such as schists, greenstone, gneiss, and quartzite, marks the top and bottom of the Kuldana Formation sandstone. Due to the rise of the Lesser and Greater Himalayas, igneous and metamorphic fragments may have formed. However, limestone fragments likely originated in the Tethyan Himalayas. This may also explain why there are so many biotite fragments present.

3.7. Paleoclimatic Conditions

The paleoclimatic condition of the Kul-dana Formation is interpreted based on the map presented by Suttner and Dutta [86]. According to an examination of the bivariant log/log plot between Qp/(F + L) and Q/(F + L), the majority of the values fall into the semi-humid domain (Figure 13b). In contrast, a few of the diagram's semiarid regions are typically suitable for these climatic conditions (Figure 13b). Comparing Qp/(F + L) with stratigraphic extents to Q/(F + L), Qp/(F + L) displays a slightly decreasing trend up section. This shows that the composition becomes less developed as it moves up. In addition, the Grantham and Velbel index of weathering (Wi = c × r) and the diagram of Syangbo and Tamrakar [88] (Figure 13c), Wi = 0 and 1 are typical field plots for sandstone.

Depending on the prevailing climatic conditions, the relief under subhumid conditions was either low to moderate or considerable. Suttner and Dutta [86] schemes may be used to infer paleo-climatic conditions from the compositional maturity of sandstone (Figure 12d). According to their QFL ratio (65:27), they were generated in semi-humid circumstances, and their compositional maturity varies from low to moderate (Table 2)

Sandstones of the Kuldana Formation include a high proportion of calcite cement (9–25%) and clay (2–11%) (Table 1). Sandstone contains carbonate grains of detrital origin, indicating that calcite and dolostone crystallized from detritus or a primary cement. Large rivers in semi-arid regions convey these carbonate pieces (Figure 14). The red color of the majority of river sediments that accumulate in semi-arid regions is a result of hematite.
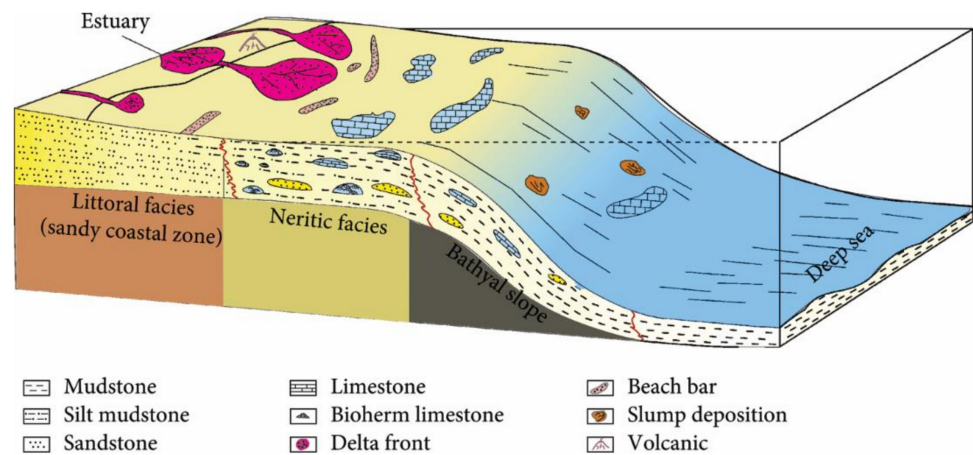
Figure 14. Depositional model of the Kuldana Formation in the area of Yadgaar section, Muzaffarabad.

Temperature and humidity may modify less-stable minerals, but excessive humidity can preserve them, according to Boggs Jr. and Boggs [89]. As a result of the slow erosion speed of grains, he predicted that chemical and physical weathering would be boosted on gentle slopes and low relief, but fast erosion would be encouraged by debris on steep slopes and high relief before its notable oxidation.

In each scenario, thrusting (Figure 15), rapid sedimentation from rivers, or climatic humidification might have countered the uplifting of the source regions (Figure 14). The feldspar granules in the Kuldana sandstone are quite numerous in comparison to the quartz grains. The reason for this is that they are able to weather the semi-humid environment. Subsequently, the Kuldana Formation was deposited primarily under semi-humid conditions (Figures 14 and 15).
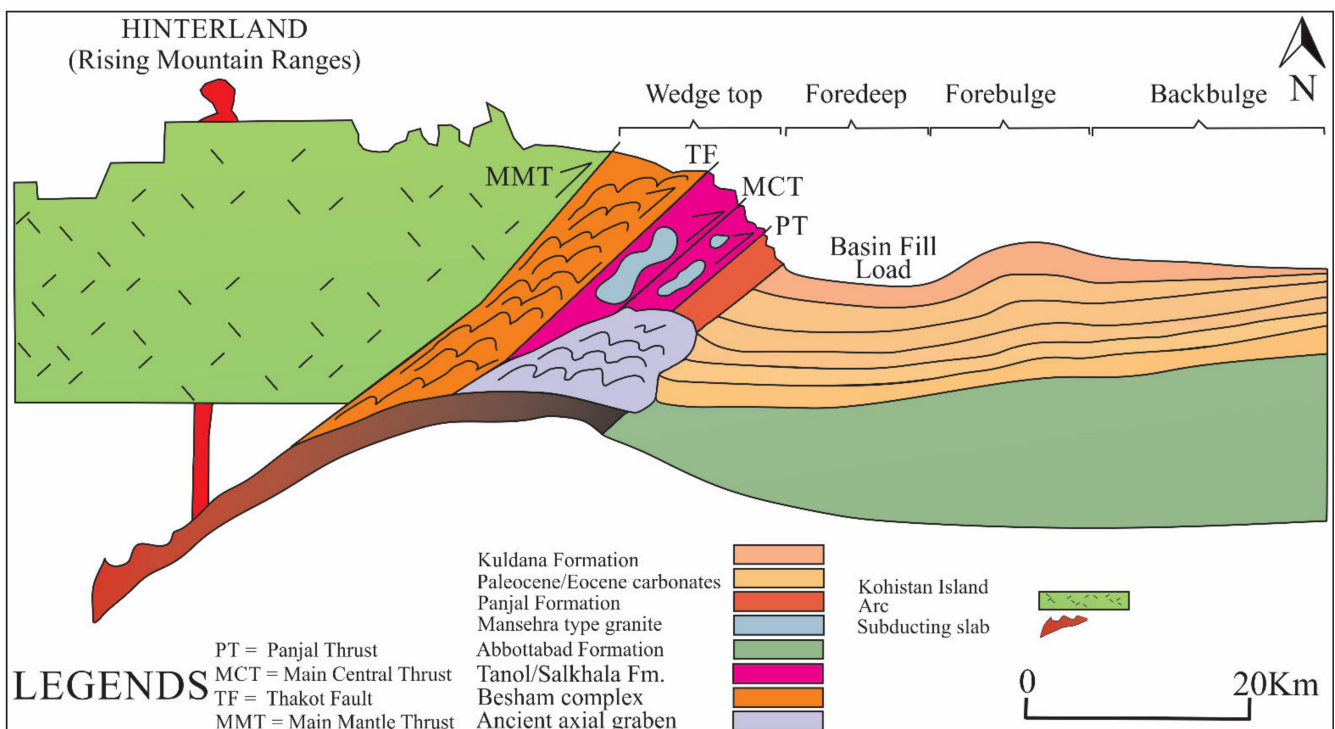
Figure 15. Hypothetical model of Indo-Eurasian continental-continental collision followed by the development of the Himalayan-Foreland Basin and the deposition of the Kuldana Formation.

In the Subathu Formation limestone, foraminifera make up a majority of the bioclasts transported by waves and tides into the coastal environment. Possible deposition of trace

fossils in littoral-subtidal zones [42]. These settings are comparable to those in the Persian Gulf, where a marine ramp environment associated with the subsidence has been identified. Foraminifera bioclasts were reported in the shallow marine Kuldana Formation of our study area and redeposited throughout the transgression and regression periods. Variegated limestone and shale facies suggest a coastal barrier and lagoonal environment, which may be linked to storm/tidal inlets. However, in the Shimla hills region, it is believed that these sediments were deposited in shelf turbidities [86] (Figure 2). In the study area, carbonate layers of the Kuldana Formation show deposition in an inner-outer ramp environment. The presence of limestone lenses indicates deposition in a neritic-bethyal setting. However, the presence of limestone lenses in sandstone and shales indicates neritic to bathyal depositional environments. The sediments are transported via a river system and ultimately deposited in a delta environment, as shown by a coarsening succession of detritus. On the top of the Subathu Formation is a forebulge unconformity, which indicates that the sediments were uplifted before the deposition of the Dagshai Formation/Murree Formation (Figure 15). Unconformity has been identified as well, which may be regional (Figure 2). Late Paleocene foreland basin sediments of the Subathu Formation are deposited in coastal off-lap environments. The sediments deposited in this foreland basin derived from both the Indian and Asian Plates [84]. Based on the detailed investigation, it is possible to conclude that the Kuldana Formation originated in a neritic-deltaic environment with a northern source (Figures 2 and 15). Previous researchers observed the presence of gastropods (*pyramidellidae*), miliolids, *Nummulites*, *Lockhartia*, ostracods, bivalves, brachiopods, *Lockharia pustulosa*, and *Neorotalia viennoti* [31,32]. They assigned the Middle Eocene age to the Kuldana Formation. However, the present study showed the presence of bivalves, brachiopods, crinoid, gastropods, *Globigerinoides* spp., *Lockhartia pustulosa*, miliolids, *Nummulites atacicus*, *Nummulites discorbina*, *Nummulites mamillatus*, *Nummulites djodjokartae*, *Nummulites vascus*, and ostracodes suggesting that the age of Kuldana Formation is Middle Eocene-early Oligocene.

4. Conclusions

The following findings are based on petrographic, sedimentological, and paleontological investigations. (1) Petrographically, the Kuldana Formation sandstone is divided into litharenite and feldspathic litharenite. The ternary diagrams QtFL and QmFLt indicate a recycled orogen provenance field for the Kuldana Formation sandstone. The Kuldana Formation clastic sediments influx derived from low and middle-to-upper rank metamorphic rocks of the Lesser and Higher Himalayas under a semiarid to semi-humid climatic conditions. (2) The Kuldana Formation limestone is characterized as mudstone, wackstone, and packstone, and it was deposited in an inner-outer ramp setting of the Ceno-Tethys Ocean. Based on the presence of micro-fossils, the Kuldana Formation has been assigned a Middle Eocene-Early Oligocene age (e.g., *Nummulites atacicus*, *Nummulites mamillatus*, *Nummulites discorbina*, *Nummulites djodjokartae*, *Nummulites vascus*, bioclast, *Lockhartia pustulosa*, gastropods, miliolids, brachiopods, *Globigerinoides* spp., crinoid, bivalves, and ostracods). The presence of fossiliferous limestone in the form of lenses revealed that they were deposited in the Neritic to Bathyal facies while the Kul-dana coarsened upward succession. The formation of the debris revealed that it was transported by the fluvial system and subsequently deposited in deltas. (3) During the initial phase of the collision between the Indian continental plate and the Asian plate, seawater fluctuations occurred. Multiple events of transgression and regression led to the redeposition of marine fossils in terrestrial sediments and the redeposition of detritus in the Ceno-Tethys Ocean, respectively. (4) During the Middle Eocene-Early Oligocene, detrital sediments from the Higher-Tethyan Himalayas were carried by large river systems into the deltaic environment of foreland basin. In the meanwhile, the same detritus was deposited in India and Nepal as shelf turbidites and tidal flat-deltaic systems. These deposits are designated as the Upper Subathu Group and the Upper Bhainskti Formation, respectively. A forebulge above

these deposits caused a regional unconformity in the Himalayan foreland regions. This unconformity is also observable in Nepal, India, and the study region of Pakistan.

References

1. Martin, C.R.; Jagoutz, O.; Upadhyay, R.; Royden, L.H.; Eddy, M.P.; Bailey, E.; Nichols, C.I.; Weiss, B.P. Paleocene latitude of the Kohistan–Ladakh arc indicates multistage India–Eurasia collision. *Proc. Natl. Acad. Sci. USA* **2020**, *117*, 29487–29494. [CrossRef] [PubMed]
2. Shah, S. Stratigraphy of Pakistan (memoirs of the geological survey of Pakistan). *Geol. Surv. Pak.* **2009**, *22*, 1–381.
3. Qasim, M.; Tanoli, J.I.; Ahmad, L.; Ding, L.; Rehman, Q.U.; Umber, U. First U-Pb Detrital Zircon Ages from Kamlial Formation (Kashmir, Pakistan): Tectonic Implications for Himalayan Exhumation. *Minerals* **2022**, *12*, 298. [CrossRef]
4. Belousov, A.; Belousova, M.; Zaw, K.; Streck, M.J.; Bindeman, I.; Meffre, S.; Vasconcelos, P. Holocene eruptions of Mt. Popa, Myanmar: Volcanological evidence of the ongoing subduction of Indian Plate along Arakan Trench. *J. Volcanol. Geotherm. Res.* **2018**, *360*, 126–138. [CrossRef]
5. Chatterjee, P.; De, S.; Ranaivoson, M.; Mazumder, R.; Arima, M. A review of the ~1600 Ma sedimentation, volcanism, and tectono-thermal events in the Singhbhum craton, Eastern India. *Geosci. Front.* **2013**, *4*, 277–287. [CrossRef]
6. Roy, B.; Roy, S.; Goyal, K.; Ghosh, S.; Sanyal, P. Biomarker and carbon isotopic evidence of marine incursions in the Himalayan foreland basin during its overfilled stage. *Paleoceanogr. Paleoclimatol.* **2021**, *36*, e2020PA004083. [CrossRef]
7. DeCelles, P.G.; Busby, C. Foreland basin systems revisited: Variations in response to tectonic settings. In *Tectonics of Sedimentary Basins: Recent Advances*; John Wiley and Sons: Hoboken, NJ, USA, 2012; pp. 405–426.
8. Mughal, M.S.; Khan, M.S.; Khan, M.R.; Mustafa, S.; Hameed, F.; Basharat, M.; Niaz, A. Petrology and geochemistry of Jura granite and granite gneiss in the Neelum Valley, Lesser Himalayas (Kashmir, Pakistan). *Arab. J. Geosci.* **2016**, *9*, 1–12. [CrossRef]
9. Li, Y.; Zhai, S.-N.; Qiu, Y.-X.; Guo, Y.-P.; Ge, X.-J.; Comes, H.P. Glacial survival east and west of the 'Mekong–Salween Divide' in the Himalaya–Hengduan Mountains region as revealed by AFLPs and cpDNA sequence variation in Sinopodophyllum hexandrum (Berberidaceae). *Mol. Phylogenet. Evol.* **2011**, *59*, 412–424. [CrossRef]
10. Acharyya, S. Evolution of the Himalayan Paleogene foreland basin, influence of its litho-packet on the formation of thrust-related domes and windows in the Eastern Himalayas—A review. *J. Asian Earth Sci.* **2007**, *31*, 1–17. [CrossRef]
11. Mughal, M.S.; Zhang, C.; Du, D.; Zhang, L.; Mustafa, S.; Hameed, F.; Khan, M.R.; Zaheer, M.; Blaise, D. Petrography and provenance of the Early Miocene Murree Formation, Himalayan Foreland Basin, Muzaffarabad, Pakistan. *J. Asian Earth Sci.* **2018**, *162*, 25–40. [CrossRef]
12. Ding, L.; Qasim, M.; Jadoon, I.A.; Khan, M.A.; Xu, Q.; Cai, F.; Wang, H.; Baral, U.; Yue, Y. The India–Asia collision in north Pakistan: Insight from the U–Pb detrital zircon provenance of Cenozoic foreland basin. *Earth Planet. Sci. Lett.* **2016**, *455*, 49–61. [CrossRef]
13. Garzanti, E.; Critelli, S.; Ingersoll, R.V. Paleogeographic and paleotectonic evolution of the Himalayan Range as reflected by detrital modes of Tertiary sandstones and modern sands (Indus transect, India and Pakistan). *Geol. Soc. Am. Bull.* **1996**, *108*, 631–642. [CrossRef]
14. Bhandari, S.; Qin, K.; Zhou, Q.; Evans, N.J. Geological, Mineralogical and Geochemical Study of the Aquamarine-Bearing Yamrang Pegmatite, Eastern Nepal with Implications for Exploration Targeting. *Minerals* **2022**, *12*, 564. [CrossRef]
15. Suresh, N.; Kumar, R. Late Quaternary Deflections of the Beas-Satluj rivers at the Himalayan mountain front, Kangra re-entrant, India: Response to fold growth and climate. *J. Asian Earth Sci.* **2020**, *191*, 104248. [CrossRef]
16. Awais, M.; Ullah, F.; Khan, N.; Ghani, M.; Siyar, S.M.; Wadood, B.; Mukhtiar, A. Investigation of reservoir characteristics, depositional setting and T–R sequences of the Lockhart Limestone of Meyal Oil Field, Pakistan: A petrophysical approach. *J. Pet. Explor. Prod. Technol.* **2019**, *9*, 2511–2530. [CrossRef]
17. Hu, X.; Garzanti, E.; Wang, J.; Huang, W.; An, W.; Webb, A. The timing of India–Asia collision onset—Facts, theories, controversies. *Earth-Sci. Rev.* **2016**, *160*, 264–299. [CrossRef]
18. Arora, B.; Unsworth, M.J.; Rawat, G. Deep resistivity structure of the northwest Indian Himalaya and its tectonic implications. *Geophys. Res. Lett.* **2007**, *34*. [CrossRef]
19. Dickinson, W.R.; Suczek, C.A. Plate tectonics and sandstone compositions. *Aapg Bull.* **1979**, *63*, 2164–2182.

20. Dickinson, W.R. Interpreting provenance relations from detrital modes of sandstones. In *Provenance of Arenites*; Springer: Berlin/Heidelberg, Germany, 1985; pp. 333–361.

21. Dickinson, W.R.; Beard, L.S.; Brakenridge, G.R.; Erjavec, J.L.; Ferguson, R.C.; Inman, K.F.; Knepp, R.A.; Lindberg, F.A.; Ryberg, P.T. Provenance of North American Phanerozoic sandstones in relation to tectonic setting. *Geol. Soc. Am. Bull.* **1983**, *94*, 222–235. [CrossRef]

22. Baig, M.S.; Munir, M.-U.-H. Foraminiferal biostratigraphy of Yadgar area, Muzaffarabad Azad Kashmir, Pakistan. *J. Himal. Earth Sci.* **2007**, *40*, 33–43.

23. Coll, X.; Roigé, M.; Gómez-Gras, D.; Teixell, A.; Boya, S.; Mestres, N. Interplay of Multiple Sediment Routing Systems Revealed by Combined Sandstone Petrography and Heavy Mineral Analysis (HMA) in the South Pyrenean Foreland Basin. *Minerals* **2022**, *12*, 262. [CrossRef]

24. Mattauer, M.; Matte, P.; Malavieille, J.; Tapponnier, P.; Maluski, H.; Qin, X.Z.; Lun, L.Y.; Qin, T.Y. Tectonics of the Qinling belt: Build-up and evolution of eastern Asia. *Nature* **1985**, *317*, 496–500. [CrossRef]

25. Zhang, G.; Zhang, B.; Yuan, X.C.; Xiao, Q. *Qinling Orogenic Belt and Continental Dynamics*; Springer Press: Beijing, China, 2001; pp. 1–855.

26. Dong, Y.; Zhang, G.; Neubauer, F.; Liu, X.; Genser, J.; Hauzenberger, C. Tectonic evolution of the Qinling orogen, China: Review and synthesis. *J. Asian Earth Sci.* **2011**, *41*, 213–237. [CrossRef]

27. Wu, Y.-B.; Zheng, Y.-F. Tectonic evolution of a composite collision orogen: An overview on the Qinling–Tongbai–Hong'an–Dabie–Sulu orogenic belt in central China. *Gondwana Res.* **2013**, *23*, 1402–1428. [CrossRef]

28. Wang, R.; Xu, Z.; Santosh, M.; Liang, F.; Fu, X. Petrogenesis and tectonic implications of the Early Paleozoic intermediate and mafic intrusions in the South Qinling Belt, Central China: Constraints from geochemistry, zircon U–Pb geochronology and Hf isotopes. *Tectonophysics* **2017**, *712*, 270–288. [CrossRef]

29. Chen, L.; Yan, Z.; Guo, X.; Fu, C. Melting of the Meso-Neoproterozoic juvenile crust for the origin of the Late Triassic Mo mineralization in South Qinling, central China: Evidence from geochronology and geochemistry of the Yangmugou deposit. *J. Asian Earth Sci.* **2019**, *174*, 109–125. [CrossRef]

30. Gingerich, P.D. Mammalian responses to climate change at the Paleocene-Eocene boundary: Polecat Bench. In *Causes and Consequences of Globally Warm Climates in the Early Paleogene*; Geological Society of America: Boulder, CO, USA, 2003; Volume 369, p. 463.

31. Meissner, C.R.; Ankary, A. *Geology of Phosphate Deposits in the Sirhan-Turayf Basin, Kingdom of Saudi Arabia*; US Geological Survey: Reston, VA, USA, 1970.

32. Latif, M. Explanatory notes on the Geology of South Eastern Hazara, to accompany the revised Geological Map. *Wien Jb. Geol. BA Sonderb* **1970**, *15*, 5–20.

33. Abbasi, I.A.; McElroy, R. Thrust kinematics in the Kohat plateau, trans Indus range, Pakistan. *J. Struct. Geol.* **1991**, *13*, 319–327. [CrossRef]

34. Środoń, J.; Drits, V.A.; McCarty, D.K.; Hsieh, J.C.; Eberl, D.D. Quantitative X-ray diffraction analysis of clay-bearing rocks from random preparations. *Clays Clay Miner.* **2001**, *49*, 514–528. [CrossRef]

35. Basu, A. A perspective on quantitative provenance analysis. In *Quantitative Provenance Studies in Italy*; Memorie Descrittive Della Carta Geologica dell'Italia; Istituto Superiore per la Protezione e la Ricerca Ambientale: Rome, Italy, 2003; Volume 61, pp. 11–22.

36. Critelli, S.; De Rosa, R.; Platt, J.P. Sandstone detrital modes in the Makran accretionary wedge, southwest Pakistan: Implications for tectonic setting and long-distance turbidite transportation. *Sediment. Geol.* **1990**, *68*, 241–260. [CrossRef]

37. Poland, M.P.; Fink, J.H.; Tauxe, L. Patterns of magma flow in segmented silicic dikes at Summer Coon volcano, Colorado: AMS and thin section analysis. *Earth Planet. Sci. Lett.* **2004**, *219*, 155–169. [CrossRef]

38. Kundu, A.; Matin, A.; Eriksson, P.G. Petrography and geochemistry of the Middle Siwalik sandstones (tertiary) in understanding the provenance of sub-Himalayan sediments in the Lish River Valley, West Bengal, India. *Arab. J. Geosci.* **2016**, *9*, 1–18. [CrossRef]

39. Kazi Tamrakar, N.; Kumar Syangbo, D. Petrography and provenance of the Siwalik Group sandstones from the Main Boundary Thrust region, Samari River area, Central Nepal, sub-Himalaya. *Bol. Geol.* **2014**, *36*, 25–44.

40. Ali, S.K.; Janjuhah, H.T.; Shahzad, S.M.; Kontakiotis, G.; Saleem, M.H.; Khan, U.; Zarkogiannis, S.D.; Makri, P.; Antonarakou, A. Depositional Sedimentary Facies, Stratigraphic Control, Paleoecological Constraints, and Paleogeographic Reconstruction of Late Permian Chhidru Formation (Western Salt Range, Pakistan). *J. Mar. Sci. Eng.* **2021**, *9*, 1372. [CrossRef]

41. Joshi, K.B.; Ray, S.; Ahmad, T.; Manavalan, S.; Aradhi, K.K. Geochemistry of meta-sediments from Neoproterozoic Shimla and Chail Groups of Outer Lesser Himalaya: Implications for provenance, tectonic setting, and paleo-weathering conditions. *Geol. J.* **2021**, *56*, 4451–4478. [CrossRef]

42. Singh, B. Evolution of the Paleogene succession of the western Himalayan foreland basin. *Geosci. Front.* **2013**, *4*, 199–212. [CrossRef]

43. Rana, R.S.; Waqas, M.; Orliac, M.; Folie, A.; Smith, T. A new basal raoellid artiodactyl (Mammalia) from the middle Eocene Subathu Group of Rajouri District, Jammu and Kashmir, northwest Himalaya, India. *Geobios* **2021**, *66*, 193–206. [CrossRef]

44. Von Eynatten, H.; Barcelo-Vidal, C.; Pawlowsky-Glahn, V. Composition and discrimination of sandstones: A statistical evaluation of different analytical methods. *J. Sediment. Res.* **2003**, *73*, 47–57. [CrossRef]

45. Garzanti, E. Petrographic classification of sand and sandstone. *Earth-Sci. Rev.* **2019**, *192*, 545–563. [CrossRef]

46. Dunham, R.J. *Classification of Carbonate Rocks According to Depositional Textures*; AAPG: Tulsa, OK, USA, 1962; pp. 108–121.

47. Folk, R.L. The natural history of crystalline calcium carbonate; effect of magnesium content and salinity. *J. Sediment. Res.* **1974**, *44*, 40–53.
48. Pettijohn, D.; Hecht, R.M.; Stimpson, D.; Van Scoyk, S. An explanation for rotor speed effects observed during sedimentation of large folded DNA molecules. *J. Mol. Biol.* **1978**, *119*, 353–359. [CrossRef]
49. Aurbach, D.; Markovsky, B.; Salitra, G.; Markevich, E.; Talyossef, Y.; Koltypin, M.; Nazar, L.; Ellis, B.; Kovacheva, D. Review on electrode–electrolyte solution interactions, related to cathode materials for Li-ion batteries. *J. Power Sources* **2007**, *165*, 491–499. [CrossRef]
50. Wang, C.; Ding, L.; Cai, F.; Zhang, L.; Li, Z.; Yue, Y. Rifting of the Indian passive continental margin: Insights from the Langjiexue basalts in the central Tethyan Himalaya, southern Tibet. *GSA Bull.* **2022**. [CrossRef]
51. Bassis, A.; Hinderer, M.; Meinhold, G. New insights into the provenance of Saudi Arabian Palaeozoic sandstones from heavy mineral analysis and single-grain geochemistry. *Sediment. Geol.* **2016**, *333*, 100–114. [CrossRef]
52. Nguidi, M.A.; Mouflih, M.; Benbouziane, A.; Kocsis, L.; El Ouariti, S.; El Boukhari, H.; Aquit, M.; Yazami, O.K. Lithofacies analysis, sedimentary dynamics and genesis of Maastrichtian-Eocene phosphorites of BouCraa deposit (southern Morocco). *J. Afr. Earth Sci.* **2021**, *177*, 104161. [CrossRef]
53. Vainauskas, J.; Topić, F.; Bushuyev, O.S.; Barrett, C.J.; Friščić, T. Halogen bonding to the azulene π-system: Cocrystal design of pleochroism. *Chem. Commun.* **2020**, *56*, 15145–15148. [CrossRef] [PubMed]
54. Bossart, P.J. Eine Neuinterpretation der Tektonik der Hazara Kashmir Syntaxis (Pakistan). Ph.D. Dissertation, ETH Zurich, Zürich, Switzerland, 1986.
55. Hu, S.; Zeng, Z.; Fang, X.; Qi, H.; Yin, X.; Chen, Z.; Li, X.; Zhu, B. Geochemical study of detrital apatite in sediment from the southern Okinawa trough: New insights into sediment provenance. *Minerals* **2019**, *9*, 619. [CrossRef]
56. Kudryashov, N.M.; Udoratina, O.V.; Coble, M.A.; Steshenko, E.N. Geochronological and geochemical study of zircon from tourmaline-muscovite granites of the Archaean Kolmozero–Voronya greenstone belt: Insights into sources of the rare-metal pegmatites. *Minerals* **2020**, *10*, 760. [CrossRef]
57. Borromeo, L.; Andò, S.; France-Lanord, C.; Coletti, G.; Hahn, A.; Garzanti, E. Provenance of Bengal shelf sediments: 1. Mineralogy and geochemistry of silt. *Minerals* **2019**, *9*, 640. [CrossRef]
58. Flügel, E.; Munnecke, A. *Microfacies of Carbonate Rocks: Analysis, Interpretation and Application*; Springer: Berlin/Heidelberg, Germany, 2010; Volume 976.
59. Adabi, M.H.; Kakemem, U.; Sadeghi, A. Sedimentary facies, depositional environment, and sequence stratigraphy of Oligocene–Miocene shallow water carbonate from the Rig Mountain, Zagros basin (SW Iran). *Carbonates Evaporites* **2016**, *31*, 69–85. [CrossRef]
60. Khan, U.; Janjuhah, H.T.; Kontakiotis, G.; Rehman, A.; Zarkogiannis, S.D. Natural Processes and Anthropogenic Activity in the Indus River Sedimentary Environment in Pakistan: A Critical Review. *J. Mar. Sci. Eng.* **2021**, *9*, 1109. [CrossRef]
61. Iannace, A.; Capuano, M.; Galluccio, L. "Dolomites and dolomites" in Mesozoic platform carbonates of the Southern Apennines: Geometric distribution, petrography and geochemistry. *Palaeogeogr. Palaeoclimatol. Palaeoecol.* **2011**, *310*, 324–339. [CrossRef]
62. Li, Y.; Huang, W.; Jiu, B.; Sun, Q.; Che, Q. Modes of occurrence and origin of minerals in Permian coals from the Huainan coalfield, Anhui, China. *Minerals* **2020**, *10*, 399. [CrossRef]
63. Rahiminejad, A.H.; Hassani, M.J. Depositional environment of the Upper Cretaceous orbitolinid-rich microfacies in the Kuh-e Mazar anticline (Kerman Province, Central Iran). *Hist. Biol.* **2016**, *28*, 597–612. [CrossRef]
64. Janjuhah, H.T.; Kontakiotis, G.; Wahid, A.; Khan, D.M.; Zarkogiannis, S.D.; Antonarakou, A. Integrated Porosity Classification and Quantification Scheme for Enhanced Carbonate Reservoir Quality: Implications from the Miocene Malaysian Carbonates. *J. Mar. Sci. Eng.* **2021**, *9*, 1410. [CrossRef]
65. Janjuhah, H.T.; Sanjuan, J.; Alqudah, M.; Salah, M.K. Biostratigraphy, Depositional and Diagenetic Processes in Carbonate Rocks from Southern Lebanon: Impact on Porosity and Permeability. *Acta Geol. Sin.* **2021**, *95*, 1668–1683. [CrossRef]
66. Abdel-Fattah, Z.A.; Kora, M.A.; Ayyad, S.N. Facies architecture and depositional development of Middle Miocene carbonate strata at Siwa Oasis, Northwestern Egypt. *Facies* **2013**, *59*, 505–528. [CrossRef]
67. Peles, F.; Sipos, P.; Győri, Z.; Pfliegler, W.P.; Giacometti, F.; Serraino, A.; Pagliuca, G.; Gazzotti, T.; Pócsi, I. Adverse effects, transformation and channeling of aflatoxins into food raw materials in livestock. *Front. Microbiol.* **2019**, *10*, 2861. [CrossRef]
68. Ebrahim, S.; Abdolhossien, A.; Ali, K.; Mohsen, S.; Seyed Mohammad, Z. Diagenetic and depositional impacts on the reservoir quality of the Upper Jurassic Arab Formation in the Balal Oilfield, Offshore Iran. *Acta Geol. Sin.* **2018**, *92*, 1523–1543. [CrossRef]
69. Chen, X.; Wang, C.; Kuhnt, W.; Holbourn, A.; Huang, Y.; Ma, C. Lithofacies, microfacies and depositional environments of Upper Cretaceous Oceanic red beds (Chuangde Formation) in southern Tibet. *Sediment. Geol.* **2011**, *235*, 100–110. [CrossRef]
70. Laschet, C. On the origin of cherts. *Facies* **1984**, *10*, 257–289. [CrossRef]
71. Ahmad, F.; Quasim, M.A.; Ahmad, A.H.M. Microfacies and diagenetic overprints in the limestones of Middle Jurassic Fort Member (Jaisalmer Formation), Western Rajasthan, India: Implications for the depositional environment, cyclicity, and reservoir quality. *Geol. J.* **2021**, *56*, 130–151. [CrossRef]
72. Janjuhah, H.T.; Alansari, A.; Santha, P.R. Interrelationship between facies association, diagenetic alteration and reservoir properties evolution in the Middle Miocene carbonate build up, Central Luconia, Offshore Sarawak, Malaysia. *Arab. J. Sci. Eng.* **2019**, *44*, 341–356. [CrossRef]
73. Wadood, B.; Khan, S.; Li, H.; Liu, Y.; Ahmad, S.; Jiao, X. Sequence stratigraphic framework of the Jurassic Samana Suk carbonate formation, North Pakistan: Implications for reservoir potential. *Arab. J. Sci. Eng.* **2021**, *46*, 525–542. [CrossRef]

74. Srivastava, V.; Singh, B. Facies analysis and depositional environments of the early Eocene Naredi Formation (Nareda locality), Kutch, Western India. *Carbonates Evaporites* **2017**, *32*, 279–293. [CrossRef]
75. Pomar, L.; Morsilli, M.; Hallock, P.; Bádenas, B. Internal waves, an under-explored source of turbulence events in the sedimentary record. *Earth-Sci. Rev.* **2012**, *111*, 56–81. [CrossRef]
76. Khatibi Mehr, M.; Adabi, M.H. Microfacies and geochemical evidence for original aragonite mineralogy of a foraminifera-dominated carbonate ramp system in the late Paleocene to Middle Eocene, Alborz basin, Iran. *Carbonates Evaporites* **2014**, *29*, 155–175. [CrossRef]
77. Brandano, M.; Tomassetti, L. MECO and Alpine orogenesis: Constraints for facies evolution of the Bartonian nummulitic and Solenomeris limestone in the Argentina Valley (Ligurian Alps). *Sedimentology* **2022**, *69*, 24–46. [CrossRef]
78. Khan, M.; Khan, M.A.; Shami, B.A.; Awais, M. Microfacies analysis and diagenetic fabric of the Lockhart Limestone exposed near Taxila, Margalla Hill Range, Punjab, Pakistan. *Arab. J. Geosci.* **2018**, *11*, 29. [CrossRef]
79. Swei, G.; Tucker, M.E. Impact of diagenesis on reservoir quality in ramp carbonates: Gialo Formation (Middle Eocene), Sirt Basin, Libya. *J. Pet. Geol.* **2012**, *35*, 25–47. [CrossRef]
80. Christ, N.; Maerz, S.; Kutschera, E.; Kwiecien, O.; Mutti, M. Palaeoenvironmental and diagenetic reconstruction of a closed-lacustrine carbonate system—The challenging marginal setting of the Miocene Ries Crater Lake (Germany). *Sedimentology* **2018**, *65*, 235–262. [CrossRef]
81. Adabi, M.H.; Zohdi, A.; Ghabeishavi, A.; Amiri-Bakhtiyar, H. Applications of nummulitids and other larger benthic foraminifera in depositional environment and sequence stratigraphy: An example from the Eocene deposits in Zagros Basin, SW Iran. *Facies* **2008**, *54*, 499–512. [CrossRef]
82. Chen, X.; Wei, M.; Li, X.; Li, M. The co-relationship of marine carbonates and evaporites: A study from the Tarim Basin, NW China. *Carbonates Evaporites* **2020**, *35*, 122. [CrossRef]
83. Schonberg, S.V.; Clarke, J.T.; Dunton, K.H. Distribution, abundance, biomass and diversity of benthic infauna in the Northeast Chukchi Sea, Alaska: Relation to environmental variables and marine mammals. *Deep. Sea Res. Part II Top. Stud. Oceanogr.* **2014**, *102*, 144–163. [CrossRef]
84. Valdiya, K. Himalayan Foreland Basin. In *The Making of India*; Springer: Berlin/Heidelberg, Germany, 2016; pp. 621–674.
85. Dickinson, W.R. Provenance and sediment dispersal in relation to paleotectonics and paleogeography of sedimentary basins. In *New Perspectives in Basin Analysis*; Springer: Berlin/Heidelberg, Germany, 1988; pp. 3–25.
86. Suttner, L.J.; Dutta, P.K. Alluvial sandstone composition and paleoclimate; I, Framework mineralogy. *J. Sediment. Res.* **1986**, *56*, 329–345.
87. Singh, B.; Singh, S.; Bhan, U. Oceanic anoxic events in the Earth's geological history and signature of such event in the Paleocene-Eocene Himalayan foreland basin sediment records of NW Himalaya, India. *Arab. J. Geosci.* **2022**, *15*, 317. [CrossRef]
88. Syangbo, D.K.; Tamrakar, N.K. Lithofacies and depositional environment of the Siwalik group in Samari-Sukaura river area, central Nepal. *Bull. Dep. Geol.* **2013**, *16*, 53–64. [CrossRef]
89. Boggs, S., Jr.; Boggs, S. *Petrology of Sedimentary Rocks*; Cambridge University Press: Cambridge, UK, 2009.